Journal of Energy Storage 28 (2020) 101077

Contents lists available at ScienceDirect

Journal of Energy Storage

journal homepage: www.elsevier.com/locate/est

Standard battery energy storage system profiles: Analysis of various applications for stationary energy storage systems using a holistic simulation framework

Daniel Kucevic [a,1,*], Benedikt Tepe [1,a], Stefan Englberger [a], Anupam Parlikar [a], Markus Mühlbauer [b], Oliver Bohlen [b], Andreas Jossen [a], Holger Hesse [a]

[a] Institute for Electrical Energy Storage Technology, Technical University of Munich (TUM), Arcisstr. 21, Munich 80333, Germany
[b] Department for Electrical Engineering and Information Technology, Munich University of Applied Sciences (HM), Lothstr. 64, Munich 80335, Germany

ARTICLE INFO

Keywords:
Battery energy storage system
Lithium ion
Storage system design
Stationary application
Operation strategy
Standard profiles

ABSTRACT

Lithium-ion batteries are used for both stationary and mobile applications. While in the automotive industry standard profiles are used to compare the performance and efficiency of competing vehicles, a similar comparative metric has not been proposed for stationary battery energy storage systems. Because standard profiles are missing, the comparable evaluation of different applications with respect to efficiency, long-term behavior and profitability is very difficult or not possible at all. This work presents a method to create these standard profiles and the results are available as open data for download. Input profiles including frequency data, industry load profiles and household load profiles are transformed into storage profiles including storage power and state of charge using a holistic simulation framework. Various degrees of freedom for the energy management system as well as for the storage design are implemented and the results are post-processed with a profile analyzer tool in order to identify six key characteristics, these being: full-equivalent cycles, efficiency, depth of cycles, resting periods, number of changes of sign and energy throughput between changes of sign. All applications examined in this paper show unique characteristics which are essential for the design of the storage system. E.g., the numbers for annual full-equivalent cycles vary from 19 to 282 and the efficiency lies between 83% and 93%. With aid of this work in conjunction with the *open data* results, users can test and compare their own cell types, operation strategies and system topologies with those of the paper. Furthermore, the storage power profiles and state of charge data can be used as a reference for lifetime and profitability studies for stationary storage systems.

1. Introduction

A high share of renewable energies poses new challenges to the power grid. Due to decreasing costs of Lithium-Ion Battery (LIB), stationary Battery Energy Storage Systems (BESSs) are discussed as a viable building block in this context. In Germany, the installed storage power with batteries increased from 126 MW in 2015 to over 700 MW in 2018 [1]. Many use cases seem to be of interest for BESSs, as summarized in a report by Eyer and Corey [2]. In particular, the provision of Frequency Containment Reserve (FCR), Peak Shaving (PS) in the industry sector and Self-consumption Increase (SCI) in the private sector are seen as the most prominent applications for BESSs [3,4]. There seems to be consensus, that these applications are the main drivers for the stationary battery storage market. However, if it comes to quantitative analyses of profitability, efficiency and aging of storage systems in a singular use case or even across applications, striking differences in numbers become apparent. In order to make single applications easier to compare, open-source available reference profiles for stationary BESS, similar to the widely used Worldwide Harmonized Light Vehicles Test Procedure (WLTP) for electric vehicles applications, are suggested herein and may help to assess the performance of BESSs.

1.1. Literature review

The state of the art of LIB based stationary BESSs is reviewed e.g. by

* Corresponding author.
E-mail address: daniel.kucevic@tum.de (D. Kucevic).
[1] These authors contributed equally to this work.

https://doi.org/10.1016/j.est.2019.101077
Received 19 August 2019; Received in revised form 8 October 2019; Accepted 13 November 2019
Available online 28 January 2020

List of Abbreviation

AC	Alternating Current
BESS	Battery Energy Storage System
C	Carbon-Graphite
DC	Direct Current
DOC	Depth of Cycle
DOF	Degrees of Freedom
E-rate	Energy Rate
ECM	Equivalent Circuit Model
EMS	Energy Management System
FCR	Frequency Containment Reserve
FEC	Full Equivalent Cycles
IDM	Intra-Day Market
IP	Input Profile
LFP	Lithium-Iron-Phosphate
LIB	Lithium-Ion Battery
NMC	Nickel-Manganese-Cobalt-Oxide
OCV	Open Circuit Voltage
PE	Power Electronics
PER	Power to energy ratio
PS	Peak Shaving
PV	Photovoltaic
SCI	Self-consumption Increase
SimSES	Simulation Tool for Stationary Energy Storage Systems
SP	Storage Profile

Diouf et al. [5] and Hesse et al. [3]. Both conclude that LIB based stationary BESSs have advantages in different stationary applications compared to alternative technologies. A more general overview of stationary storage systems, including other storage technologies, is given by Palizban and Kauhaniemi [6], Resch et al. [4] and Dunn et al. [7]. All authors highlight the high efficiency of LIB-based BESSs, but the numbers, due to different definitions, vary from less than 90% up to 94%. A systematic review of Energy Management System (EMS) for BESS was published by Weitzel and Glock [8]. The placement in distribution grids of stationary BESS is summarized in the review of Das et al. [9]. An example for optimized placement using simultaneous perturbation stochastic approximation method was published by Carpinelli et al. [10].

Regarding the provision of FCR with BESS, a number of papers have been published in the past. Specifically for several techno-economic evaluations different approaches exist [11–15]. Münderlein et al. [16] analyzed a large scale 5 MW and 5 MWh BESS in the FCR market. Apart from the fact that the focus of the individual authors is different, it is noticeable that many different numbers exist. For example the authors in [16] determined 147 Full Equivalent Cycles (FEC) per year, while the numbers of FECs in [13] varies from 207 to 254 per year.

In the case of SCI, many publications with various objectives exist. The publications can be split into economic analyses [17–20] and sizing of the system [21–23]. All authors conclude that a BESS for SCI can be

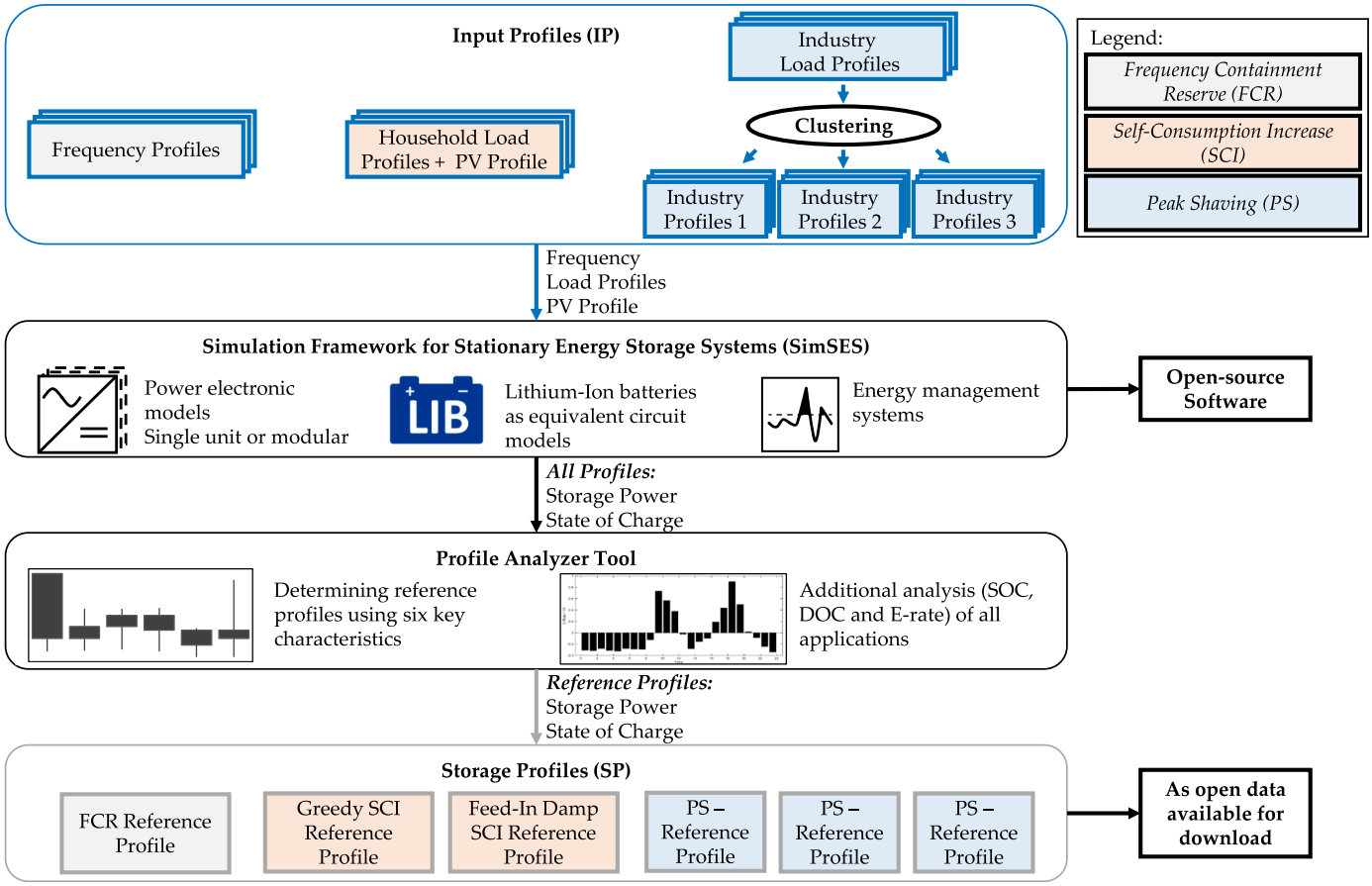

Fig. 1. Graphical overview of this work. The input profiles including frequency data, industry load profiles and household load profiles are transformed into storage profiles including storage power and state of charge using the simulation framework SimSES. The selection of suitable reference profiles is done with a profile analyzer tool developed as part of this publication.

economically viable, if the Photovoltaic (PV) unit and the storage capacity are dimensioned correctly. However, a wide variety of input data and parameters for the storage system (e.g. the efficiency for the LIB varies from 95% in [21] to 98% in [20]) are used in the publications, which makes comparability difficult.

For industry PS BESSs with LIB, fewer publications are available, in contrast to SCI BESSs. Martins et al. [24] present an approach for an optimal component sizing and the authors also performed an economic analysis. They showed in a case study that the number of FEC varies between 1 and 51 per year. Dagdougui et al. [25] show an EMS for a real world example. They optimized the size of a PS BESS for a university campus. It has been found that in this example the economically optimal storage capacity is 436 kWh. Telaretti and Dusonchet [26] concucted an economic analysis and compared the use of LIB in PS applications with three other electrochemical technologies: Lead-acid, flow based batteries and sodium-sulphur.

Although each author makes different assumptions and sets the focus differently, the results, some of which are very diverse, indicate that *open data* available standards for stationary BESS are desired.

1.2. Scope of this work

This work presents a method to create standard Storage Profile (SP) including the storage power and the SOC from Input Profile (IP) including frequency data, industry load profiles and household load profiles. The IPs are transformed into SPs by using the holistic simulation framework Simulation Tool for Stationary Energy Storage Systems (SimSES). Various Degrees of Freedom (DOF) for the EMS and the system configuration are implemented in SimSES and the results are post-processed with a newly developed profile analyzer tool in order to identify some key characteristics, such as efficiency, FEC or Depth of Cycle (DOC).

Fig. 1 shows the scope of this paper in detail. The simulation framework, as well as the results, including SPs and the SOCs, are made available as open-source. The results are available in one second resolution and may facilitate the comparison of the same applications among each other in the future. As an example, own system configurations or developed EMS can be compared with the numbers of this paper. Furthermore, the open-source available data can be used as a reference for lifetime and profitability studies for LIBs.

1.3. Paper structure

Section 2 gives an overview of the origin of the IPs and the pre-processing of the raw data sets. Section 3 describes the simulation tool SimSES with various DOFs and the developed EMS. In the remaining part of the paper, the SPs are analyzed (Section 4) and the choice of the reference profiles (Section 5) is described. Section 6 gives an outlook to future work and concludes this paper.

2. Profile data and preparation

In this chapter, the database of household load profiles, industry load profiles and frequency data is explained (Section 2.1). Herein, the data sources and time frames are described. The processing of this data is covered in Section 2.2. Subsequently, the normalization of the profiles is illustrated, which is required for comparison of data (Section 2.3). Finally, Section 2.4 covers the clustering of profiles.

2.1. Data basis

The creation of reference load and storage profiles demands a database that is sufficiently detailed to represent the specific type of profile. As described in Section 1, this paper considers three different applications of storage systems: SCI in the private sector, PS in the industry sector and the provision of FCR. These three applications require specific data with specific resolution which is displayed in Table 1.

Table 1
Storage applications, the data basis, the required data and the data resulution used in this work.

Application:	FCR	SCI	PS
Database	5 years of Frequency Data	74 yearly load profiles & one PV generation profile	36 yearly industry load profiles
Data resolution (raw data)	1 s	1 s	15 min
Data resolution (simulation)	1 s	1 s	1 s

Firstly, high resolution frequency data is required to investigate the storage application of FCR [27]. This one second resolution data for the years 2013 until 2017, that can be measured at every socket within the synchronous grid of Continental Europe, is provided by the transmission system operator *50hertz Transmission GmbH* [27]. Exemplary data of the year 2017 is shown in Fig. A.12.

The analysis of the performance of SCI requires household load profiles and photovoltaic generation profiles. Therefore, 74 load profiles published by the *HTW Berlin* are used [28]. Moreover, one photovoltaic profile measured at *TU Munich* which was already published in several previous papers [17,19,29] was used. These profiles also have a resolution of one second. To perform PS with a storage system, industry load profiles are needed. Therefore, 36 annual industry profiles with a resolution of 15 min are gathered within the *EffSkalBatt* project[2]Frequency data, household load profiles and industry load profiles work as IPs for SimSES (see Fig. 1) which will be explained in Section 3.

2.2. Data processing

The gathered data of frequency, load and photovoltaic profiles is processed before using them within the simulations. The frequency data for performing FCR with a BESS contains some doubtful values ($<$ 49 Hz or $>$ 51 Hz). All such values were replaced by linear interpolation of frequencies before and after. As the raw industry load profiles used for PS have a resolution of 15 min, this data is transformed into profiles with a resolution of one second. For this reason, the following procedure is applied to create second-based profiles: First, the 15-min points are interpolated linearly to create points based on minutes. Then random numbers are build, which replace each interpolated value. Each random number lies within the coefficient of variation of 0.25 of the normal distribution with a mean of the interpolated value. Afterwards, the minute-based values are interpolated linearly again to reach a second-based load profile.

This procedure only estimates the high-resolution load profile. Possible load peaks that just appear for a few seconds are not taken into account. Those short peaks are crucial when regarding battery lifetime and safety [30,31]. Within the application of PS the presented procedure to reach second-based load profiles is sufficient, as the storage system only has to provide the required energy when peaks appear as long as the storage's power is sufficient. The required energy can also be extracted from the 15-min load profile. Moreover, the yearly industry load profiles are chopped to match a Monday to Sunday pattern.

2.3. Normalization

After the aforementioned data pre-processing, the industry profiles are normalized, which is necessary for a comparison of profiles. The

[2] EffSkalBatt Project: Efficient scalable system technology for stationary storage systems. Research project funded by the Federal Ministry for Economic Affairs and Energy (BMWi) with grant number 03ET6148 (http://www.ees.ei.tum.de/en/research/effskalbatt/).

industry profiles are normalized to their maximum value within the year. Thus, the maximal value of each profile is one and the minimal value is zero. This normalization method on each highest peak might differentiate profiles that are similar except for their highest peaks. If only those load profiles were compared, this method would not be appropriate. However, regarding the application of peak shaving, which concentrates on the highest peaks, those profiles are very different. With this method of normalization users can compare their own profiles with the published ones and add their profiles to the simulation. The raw data of household load profiles is already normalized to each maximal value.

2.4. Clustering

Prior to the creation of reference profiles from the pre-processed data, a clustering of the different groups of profiles is considered. This is due to the fact that, for example, the industry profiles do not all have homogeneous curves. Thus, similar profiles are clustered into groups. The clustering is performed using the simulation platform MATLAB® and the clustering algorithm k-means with euclidean distances as measure of dissimilarity [32]. The k-means algorithm was chosen, as it appears to be the most prominent one when comparing electric load profiles [33–35]. Other possible clustering methods would have been the hierarchical clustering or self-organizing maps, as published in [36] and [37].

When comparing the household load profiles to each other, they appear very homogeneous. The average value of each yearly household load varies between 0.6% and 4.4% of its yearly maximum value. In addition, the mean absolute deviations of the profiles' offsets lie between 0.8 and 3.6 percentage points. In contrast to that, the industry load profiles show bigger variations. The mean load of each profile lies between 30% and 75% of the profile's yearly maximum. Thus, the industry profiles' offsets are substantially higher than the households' ones due to their increased base load. The industry loads' mean absolute deviations vary between 0.8 and 23 percentage points.

As a consequence, the industry load profiles are clustered into three different groups while the household load profiles remain in one group. The number of three is chosen because three is the best compromise between differentiation and effort.

Cluster 1 and 3 have an average load of 70% to 80% during the day and a base load of 20 to 30% at night but are shifted by a few hours. During the weekend, Cluster 1 exhibits the typical nightly base load while the load of Cluster 3 only sees the base load on Saturdays. In comparison, Cluster 2 does not have a typical day vs. night load profile. During working days the load varies between 50% and 100% and on weekends between 35% and 70%.

3. Simulation framework for stationary energy storage systems

To generate battery profiles and SPs from the IPs in Section 2 the software SimSES was used. SimSES is a modular object-oriented simulation tool, which was initiated by Naumann and Truong [38] and is now being further developed by the authors. The software allows the flexible usage of components, such as the power electronic or battery cell, of a BESS. The software code is programmed in MATLAB®, but will be converted to Python in the future and made available completely open-source. The current open-source version, including the simulation scripts for this publication and a link to the code of SimSES can be found online[3]. In this chapter the structure of SimSES (Section 3.1), the developed operation strategies (Sections 3.2–3.4) as well as the components used (Section 3.5) will be described.

3.1. Simulation structure

In SimSES the battery is implemented as a single-cell Equivalent Circuit Model (ECM). The terminal voltage U_T of each cell is calculated from the Open Circuit Voltage (OCV) and the voltage drop (overvoltage) ΔU across the series resistance R_i, due to the current I (Eq. 1). The OCV is a function of the SOC. The series resistance R_i is dependent on the current direction sign sgn(I), the temperature T and the SOC.

$$U_T = U_{OCV} - \Delta U = U_{OCV} - I \cdot R_i(SOC, sgn(I), T) \tag{1}$$

The Power Electronics (PE) efficiency is modeled as a function which relies on the absolute output power $|P_{Storage}|$, the rated power P_{Rated} and the current direction sgn(I) (Eq. 2). Fixed PE efficiency values or other functions, for example based on own investigations, can be modeled in SimSES as well. Beside the Direct Current (DC)/Alternating Current (AC) link, the PE can also include a transformer model.

$$\eta_{PE} = f\left(|P_{Storage}|, P_{Rated}, sgn(I)\right) \tag{2}$$

The core of SimSES is the EMS, which allows to simulate various tasks for a stationary BESS. As described in Section 1, the focus of this work is on the single-use applications FCR, SCI and PS.

3.2. Frequency containment reserve

The EMS for providing FCR in SimSES was developed according to the German regulatory framework [39,40]. The requested charging and discharging power $P_{Storage,set}$ is proportional to the frequency deviation Δf and is dependent on the prequalified power P_{PQ}, which has a minimum of 1 MW (Eq. 3). Below 49.8 Hz or above 50.2 Hz $P_{Storage,set}$ is set to $\pm P_{PQ}$.

$$\begin{aligned} P_{Storage,set}(t) &= P_{PQ} \cdot \frac{\Delta f(t)}{0.2\,Hz} && \text{for} \quad |\Delta f| \le 0.2\,\text{Hz} \\ P_{Storage,set}(t) &= P_{PQ} && \text{for} \quad \Delta f > +0.2\,\text{Hz} \\ P_{Storage,set}(t) &= -P_{PQ} && \text{for} \quad \Delta f < -0.2\,\text{Hz} \end{aligned} \tag{3}$$

If the SOC falls below a predefined lower limit (SOC_{low}) or it exceeds an upper limit (SOC_{high}) the BESS in these simulations charges or discharges by trading energy on the electricity market, in particular the Intra-Day Market (IDM) [14]. Due to the current legal interpretation (May 9, 2019) [41], a BESS in the FCR market has to ensure that at all times the full prequalified power P_{PQ} can be provided for 15 min as long as the frequency f is in normal progression. The normal progression means that the frequency deviation Δf is continuously less than 50 mHz or none of the following criteria is met:

- $|\Delta f| >$ 200 mHz
- $|\Delta f| >$ 100 mHz for more than 5 min
- $|\Delta f| >$ 50 mHz for more than 15 min

The SOC limits also depend on the prequalified power P_{PQ} and the storage capacity E_{BESS}, and are calculated according to Eq. 4.

$$SOC_{high} = \frac{E_{BESS} - 0.25\,h \cdot P_{PQ}}{E_{BESS}} \quad SOC_{low} = \frac{0.25\,h \cdot P_{PQ}}{E_{BESS}} \tag{4}$$

To reach these limits as infrequently as possible, the efficiency must be taken into account and therefore the SOC setpoint is above 50% (Eq. 5). The mean efficiency η_{mean} is calculated at the beginning of the simulations and is dependent on the efficiency of the battery and PE.

$$SOC_{Offset} = 0.5 \cdot \frac{\left(1 - \eta_{mean}^2\right)}{\left(1 + \eta_{mean}^2\right)} \quad SOC_{Set} = 50\% + SOC_{Offset} \tag{5}$$

Additionally to the SOC setpoint shift, the regulatory framework in Germany allows three different DOFs:

[3] http://www.ees.ei.tum.de/simses/

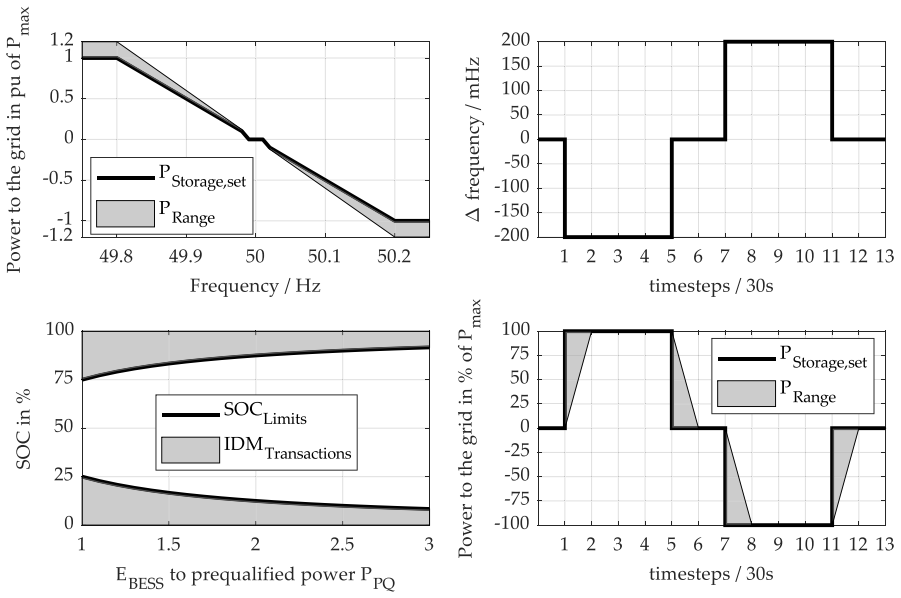

Fig. 2. Degrees of freedom and the SOC limits, depending on the prequalified power P_{PQ}. The top left subfigure shows the frequency dead band and the possible overfulfillment. The two subplots on the right show the slope and the bottom left subfigure shows the SOC limits.

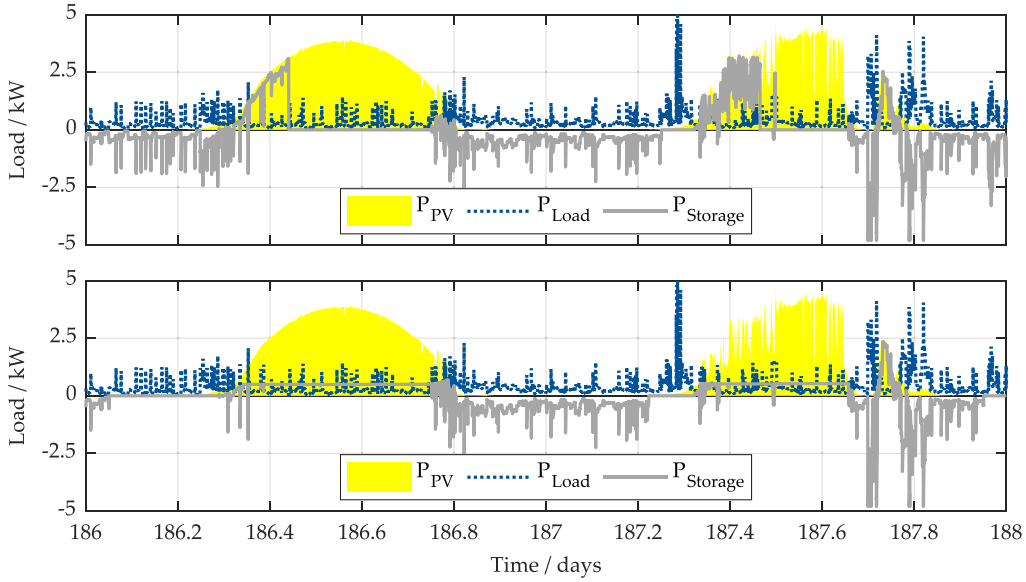

Fig. 3. Operation Strategies (top=*greedy*, bottom=*feed-in damping*) for the Residential Photovoltaic Battery Storage System. The shaded yellow area shows the generation of the PV power system, the blue line shows the load of the household and the gray line shows the storage power (positve=charging). (For interpretation of the references to color in this figure legend, the reader is referred to the web version of this article.)

- *Frequency dead band:* In the frequency range between 49.99 Hz and 50.01 Hz, the output power of the BESS can be set to 0 MW and must not follow the frequency derivation according to Eq. 3.
- *Overfulfillment:* It is allowed to overfulfill the requested power (Eq. 3) by 20 %.
- *Slope*: The requested FCR power (Eq. 3) must be provided within 30 s or earlier. Therefore, the slope of the provided FCR power can be adjusted within the time interval of 30 s allowing to control the charging or discharging rate.

In SimSES all DOF are only used, if the requested power either brings the SOC closer to optimum again or at least not further away. All degrees of freedom as well as the SOC limits, depending on the prequalified power P_{PQ}, are shown schematically in Fig. 2.

3.3. Residential photovoltaic battery storage system

In SimSES two different operation strategies for the SCI of BESS are implemented: *Greedy* and an extension of *feed-in damping* based on Zeh and Witzmann [29].

Greedy

The EMS for the greedy algorithm works with a simple comparison between the generation of the PV power system P_{PV} and the consumption by the household P_{load} at each timestep. Whenever a solar surplus occurs ($P_{PV} > P_{load}$), the BESS is charged and vice versa (Eq. 6). This conventional strategy is shown in Fig. 3 (top). These summer days show that the BESS is fully charged at around 9AM, which causes a rapid rise of the power fed into the grid. Another disadvantage of this strategy is the high charging power, which may lead to a faster decrease of the LIB capacity due to an increase of lithium plating as described in [30].

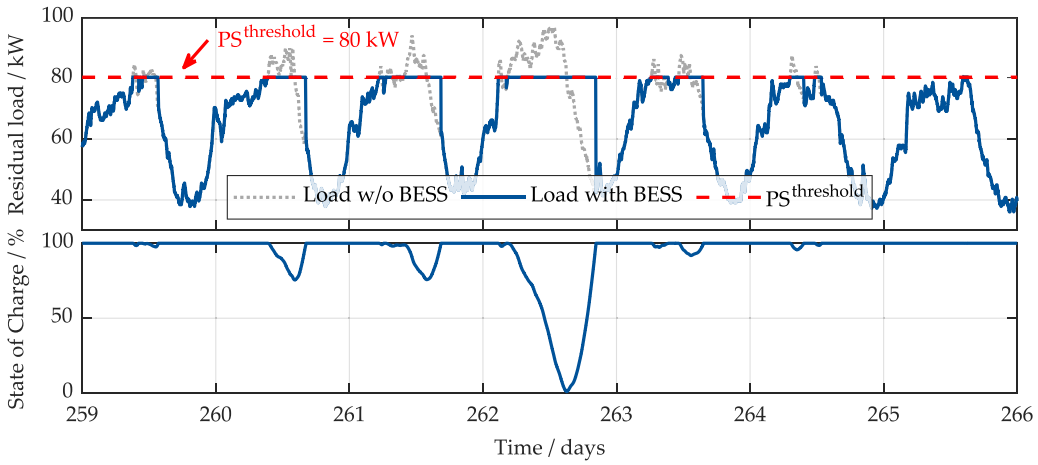

Fig. 4. Exemplary week of an industry load profile and its optimized PS threshold $PS^{threshold}$ following the PS operating strategy. The power above the threshold is provided by a stationary BESS. The solid blue line shows the industry load profile with the PS BESS. The associated SOC is illustrated at the subplot at the bottom. (For interpretation of the references to color in this figure legend, the reader is referred to the web version of this article.)

$$P_{Storage} = P_{PV} - P_{load} \quad (6)$$

Feed-in damping

In order to reduce the maximum power fed into the grid, a nearly constant BESS charging power $P_{Storage,\,Ch}$ during the whole daytime is calculated by the EMS. Reducing the maximum feed-in power allows for a higher self-consumption rate, if the maximum feed-in power is limited by the distribution grid operator as described in [19]. If a surplus ($P_{PV} > P_{load}$) occurs, the charging power $P_{Storage,Ch}$ is calculated by dividing the remaining battery capacity $E_{BESS,re}$ by the predicted remaining time t_{re}, until the load is higher than the PV generation, and the mean efficiency η_{mean} of the BESS (Eq. 7).

In this work, a perfect foresight for the duration of PV generation is assumed. If there is a higher consumption by the household than generation by the PV power system, the BESS is discharged. Fig. 3 (bottom) displays this operation strategy. In contrast to the *greedy* algorithm, the charging power is constant during the whole first day. The second day shows a more cloudy day. The remaining time t_{re} at this day is smaller than in day 1, so according to Eq. 7 the charging power $P_{Storage,ch}$ is higher. In addition, the second day also shows that after the PV generation surpasses load again ($P_{PV} - P_{load} > 0$), the remaining time t_{re} is recalculated. In this case, the storage can be charged with the full power, due to the short remaining time t_{re}.

$$P_{Storage,ch} = \frac{E_{BESS,re}}{t_{re} \cdot \eta_{mean}} \quad \text{for} \quad P_{PV} > P_{load} \quad (7)$$

3.4. Peak shaving storage system

Motivated by a tariff system consisting of an energy and a power related component, the storage application PS has the goal to minimize the maximum power peak value within a defined accounting period. Particularly large electricity consumers (annual demand $>$ 100 MWh (in Germany)) can reduce the peak power provided by the power grid, which directly results in reduced operating expenses in form of reduced grid charges [42].

In order to reduce the power at the point of common coupling, the excess demand has to be covered by another power providing unit, such as a BESS. The BESS is used to decouple the supply and demand over a specified time. To maximize the benefit of the application, it is important that the dimensioning of the storage system is the best possible match for the power demand curve. Similar to other publications [43–45], a two-step approach of a linear programming algorithm and SimSES is applied.

First, a pre-processing linear optimization algorithm is used to minimize the power value for the peak shaving threshold $PS^{threshold}$, while it complies with the necessary constraints, such as meeting the power demand, and satisfying the energy and power specifications of the BESS. Depending on the shape of the load profile, the resulting value of the power threshold varies. Secondly, the resulting peak shaving threshold is used as an input parameter for the operation strategy within SimSES. This operation strategy works as follows: as soon as the power at the point of common coupling (from the grid) is above the specified threshold, the additionally required power is provided by the BESS, as illustrated in Fig. 4. In addition, the BESS will recharge if the power value is below the previously determined optimal peak shaving threshold. This ensures that the charging of the storage system does not cause the exceedance of the threshold.

Through a close coordination of the two simulation tools in the chosen two-stage approach, both a near optimal PS threshold is found and simultaneously, the detailed technical specifications of the BESS are simulated via SimSES.

Table 2
Parameters of the simulated Lithium-ion cells. Celltype 1 is a Lithium-ion battery with a Lithium-Iron-Phosphate (LFP) cathode and a Carbon-Graphite (C) anode. Celltype 2 is a Lithium-ion battery with a Nickel-Manganese-Cobalt (NMC) and a Carbon-Graphite (C) anode.

Parameter	Unit	Cell 1 [46]	Cell 2 [50]
Cell Identification	-	US26650FTC1	IHR18650A
Manufacturer	-	Murata	E-ONE Moli Energy Corp.
Chemistry	-	LFP:C	NMC:C
Capacity	mAh	2850	1950
Max. Charge Current	A	2.85	2
Max. Discharge Current	A	20	4
Nominal Voltage	V	3.2	3.7
Voltage Range	V	2 - 3.6	3 - 4.2

3.5. Simulation parameters

The battery cell used in all simulations was a LIB with a Lithium-Iron-Phosphate (LFP) cathode and a Carbon-Graphite(C) anode [46]. It is worth to mention, that other LIB types are also implemented in the simulation tool but the LFP:C cell is a promising battery chemistry for stationary applications, because of its characteristics such as high thermal stability, long cycle as well as calendar lifetime [3,47,48]. The parameterization of the ECM for the simulated LFP:C cell was carried out by Naumann [49].

To analyze the effects of cell selection, another cell with a Nickel-

Table 3
Summary of the parameters for the simulation of the three applications with SimSES.

Application:	FCR	SCI	PS
Battery	LFP:CNMC:C	LFP:C	LFP:C
Storage Capacity	1.6 MWh	5 kWh	100 kWh
Max. Power	1.6 MW	5 kW	40 kW
PE mode	modular single unit	single unit	single unit
PV Power	-	5 kWp	-
Operation Strategy	15 min criteria	greedy feed-in damp	simple
PER	0.7	-	-
IDM Power	0.48 MW	-	-
PS-Limit	-	-	variable 62 - 92%

Manganese-Cobalt-Oxide (NMC) cathode and a C anode [50] was also simulated in the FCR application. The characterization of this cell is based on the work of Schuster [51]. The self-discharge and the temperature dependency of the cell is neglected in this work. Table 2 summarizes the parameters of these battery cells.

The PE is implemented as a function, which shows a high efficiency above 10% of the rated power P_{Rated} (Eq. 8). Exemplary values used for a high efficiency PE are $k = 0.0345$; $p_0 = 0.0072$, according to Notton et al. [52]. Here η_{PE} is independent of the direction of the power flow and no hysteresis is implemented. The maximum efficiency is observed at $0.46 \cdot P_{Rated}$ with an efficiency $\eta_{PE} = 96.9\%$.

$$\eta_{PE} = \frac{\frac{|P_{Storage}|}{P_{Rated}}}{\frac{|P_{Storage}|}{P_{Rated}} + p_0 + k \cdot \left(\frac{|P_{Storage}|}{P_{Rated}}\right)^2} \quad (8)$$

Frequency Containment Reserve

As already shown by others [3,13,14], a BESS in the FCR market is mostly in part-load operation. In order to achieve a high part-load efficiency, we minimized the inverter losses by modularization of the PE-unit into three identical smaller units based on the work of Schimpe et al. [53]. At 80% power of the rated power of PE unit 1, PE unit 2 starts to work. At 80% power of the rated power of PE unit 1 and PE unit 2, PE unit 3 starts to work. There is no hysteresis included in the simulations, which means that the switch-off values are equal to the switch-on values. According to the modeled PE efficiency, the average efficiency of this PE combination is 96%. This PE combination, together with the simulated LIB ($\eta_{LIB} = 96\%$), results in an SOC shift, according to Eq. 5, of 54%.

In this work the BESS capacity E_{BESS} is set to 1.6 MWh with a maximum power of 1.6 MW. The prequalified power P_{PQ} is 1.12 MW, which results in a Power to Energy Ratio (PER) of 0.7. Thus, the available IDM power is 30% of the total BESS power. The losses of a transformer model for a potential integration to higher grid voltage levels, which would be necessary having a 1.6 MW / 1.6 MWh storage, are neglected.

Residential Photovoltaic Battery Energy Storage System

To ensure comparability, the simulations are carried out with a fixed annual household load $E_{load,a}$ of 5,000 kWh, which rounded corresponds to the mean of the IP. According to the work of Weniger et al. [21] and Hoppmann et al. [54], the PV system and the BESS can be operated economically in the ratio 1:1:1. An annual household load $E_{load,a}$ of 5,000 kWh leads to a PV peak power of 5 kWp and a BESS capacity E_{BESS} of 5 kWh.

Peak Shaving Storage System

For the PS application, 36 anonymized annual load profiles from commercial electricity consumers are utilized. In order to generate comprehensive standardized profiles, all normalized load curves are scaled to a peak power of 100 kW (see Section 2.3). The BESS is characterized by a nominal energy content of 100 kWh. We assume that 100% of the nominal storage energy and a rated power of 40 kW for the system's PE unit (consisting of a single inverter) can be used to operate the application.

Table 3 summarizes the parameter set for each simulation in SimSES. Other components, such as

- a transformer model for a potential integration to higher grid voltage levels,
- a cell-to-cell connection resistance,
- a battery management system,
- a thermal model for each cell as well as a thermal model for the whole storage system,
- an aging model of the battery cell as well as all other subcomponets,

were neglected in this paper, but can be modeled in principle in SimSES.

4. Storage profile analyzer tool

One goal of this work is finding reference SPs for the different storage applications. Therefore, groups of SPs were created using the software SimSES. In this chapter, a storage profile analyzer tool is presented which aims to extract the reference SP for each of the groups. The idea and the reasons for the analyzer tool are described in Section 4.1. Afterwards, the different characteristics are explained in Section 4.2. Finally, the determination of reference profiles from the characteristics is described in Section 4.3. Moreover, Appendix B provides some further analysis of the SPs including the distribution of the energy rate (E-rate). The E-rate at each timestep i is defined according to Eq. 9.

$$E_{rate,i} = \frac{P_{Storage,i}}{E_{BESS}} \quad (9)$$

4.1. Reasons for the storage profile analyzer tool

The extraction of a reference SP can be done in different kind of ways. Taking the mean SP by calculating the mean of all the SPs for the different applications is one option. This would lead to a smoothing of the profiles. Distinctive peaks would be neglected and the profiles would not be representative anymore. A more viable approach is the selection of one SP as reference SP for each application. Here, a median profile has to be found which represents the group of profiles. This selection is done using the storage profile analyzer tool. The tool takes the load of the storage and SOC data as input variables and outputs the characteristics described in the following subsection.

4.2. Extracted characteristics from profiles

To better analyze and compare the storage load profiles, six characteristics were defined which are distinctive for the profiles of the different applications. Those six characteristics aim to represent the differences within the storage applications.

1. Number of full equivalent cycles (FEC)

The total number of cycles FEC_{year} within the year is calculated by dividing the positive energy throughput E^{pos}_{year} by the storage capacity E_{BESS} (Eq. 10). The FEC_{year} varies between the applications and affects the aging of the battery [30].

$$FEC_{year} = \frac{E^{pos}_{year}}{E_{BESS}} \quad (10)$$

2. Efficiency (η_{BEES})

The efficiency of the analyzed storage η_{BEES} is calculated by counting the yearly energy that is extracted from the storage system E^{neg}_{year} divided by the energy that is stored in the storage system E^{pos}_{year}. The SOC at the beginning of the year and at the end of the year is taken into account as well (Eq. 11). This characteristic displays the losses in the storage system

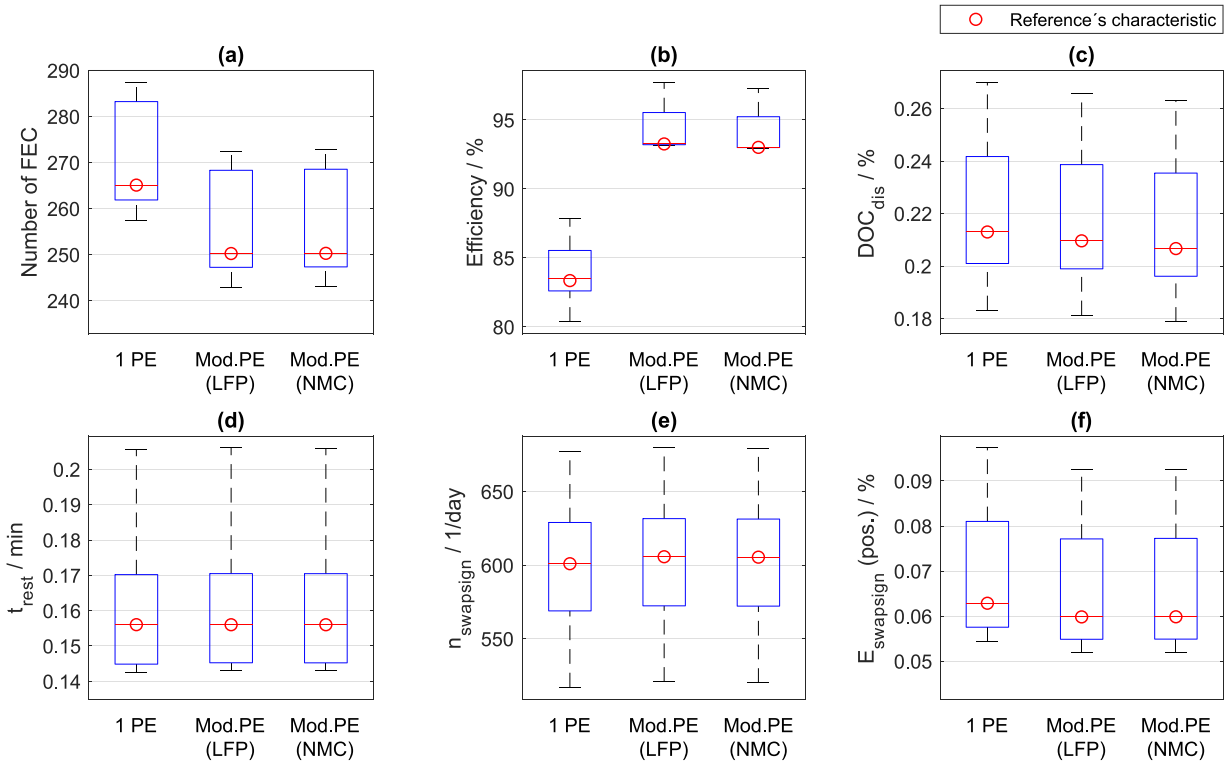

Fig. 5. Characteristics of a BESS providing FCR. The left box in each plot shows a BESS with one PE unit and a LFP:C cell. The center one in each plot shows a BESS with three modular PE units and a LFP:C cell and the right box in each plot shows a BESS with three modular PE units and a NMC:C cell.

while operating in the specific application. For the calculation of the efficiency the surrounding temperature and the thermal management are not taken into account.

$$\eta_{\mathrm{BEES}} = \frac{|\mathrm{E}^{\mathrm{neg}}_{\mathrm{year}}|}{\mathrm{E}^{\mathrm{pos}}_{\mathrm{year}} - [\mathrm{SOC}_{\mathrm{end}} - \mathrm{SOC}_{\mathrm{start}}] \cdot \mathrm{E}_{\mathrm{BESS}}} \tag{11}$$

3. Cycle depth in discharge direction (DOC_{dis})

The average DOC in discharge direction is calculated by using the SOC data of the current profile. This characteristic describes how deep the battery is discharged before recharging it. A higher DOC may lead to a higher cyclic aging of the battery [55]. To enable a comparison between the applications (different capacities) the DOC is measured in percentage of the total battery capacity. In SimSES a half-cycle detector is implemented. The beginning of the half-cycle is a change from charging respectively resting to discharging. Analogously the end is at every change from discharging to charging or if the BESS reaches an SOC of 0%. Then the DOC is calculated by subtracting the SOC at the beginning and the SOC at the end of the half-cycle (see Eq. 12). Taking only the change from discharging to charging leads to a dependency of the DOC on the resolution. Many small changes of load might outweigh larger trends.

$$\mathrm{DOC}_{\mathrm{dis}} = \mathrm{SOC}_{\mathrm{cycle,start}} - \mathrm{SOC}_{\mathrm{cycle,end}} \tag{12}$$

4. Number of changes of sign ($n_{swapsign}$)

Depending on the storage application, the SP might change from charging to discharging and vice versa very often or just a few times per day. Those changes of signs activate the power electronics. When analyzing experimental SPs the user of the storage profile analyzer tool would have to define a threshold value to prevent faults of noise when the SP is close to zero. As the simulated SPs do not show the noise, a threshold value is not necessary.

5. Length of resting periods (t_{rest})

As the BESS is not used continuously over time, the length of resting periods represent another characteristic. During those times, the BESS is neither charged nor discharged. Here, the average value of resting period length in minutes is calculated. Depending on the application the length of those resting periods may vary significantly. This characteristic is chosen because auxiliary users can be turned off and other applications can be performed during long resting periods.

6. Energy between changes of sign ($E_{swapsign}$)

Another chosen characteristic is the energy that is charged or discharged between changes of signs, respectively. The amount of the energy is normalized to the battery's capacity and thus comparable between the different applications with different capacities. Here charged and discharged energy are calculated separately.

4.3. Determination of reference profiles

The storage profile analyzer tool extracts the different characteristics from each of the profiles of the specific group of SPs. For each application the characteristics can then be displayed in boxplots to visualize the spread and show the median values.

To determine each reference profile the percentage error δ of each profile's characteristic to the median characteristic is calculated (Eq. 13). This is done by subtracting the median of the characteristic $\widetilde{K}_j$ from the profile's characteristic K_j, dividing the difference by the median of the characteristic and multiply the result with 100. Here, *i* is the number of the profile and *j* the number of the characteristic.

Afterwards, the root mean square percentage error (RMSPE) is identified for each profile (Eq. 14). This is done by taking the sum of the absolute percentage errors, dividing it by six (six characteristics), squaring it and extracting the root. This way all characteristics are weighted equally.

$$\delta_{\mathrm{i,j}} = \frac{\mathrm{K_{i,j}} - \widetilde{\mathrm{K}}_{\mathrm{j}}}{\widetilde{\mathrm{K}}_{\mathrm{j}}} \cdot 100 \tag{13}$$

$$\mathrm{RMSPE_i} = \sqrt{\left(\frac{\sum_{j=1}^{6} |\delta_{i,j}|}{6}\right)^2} \tag{14}$$

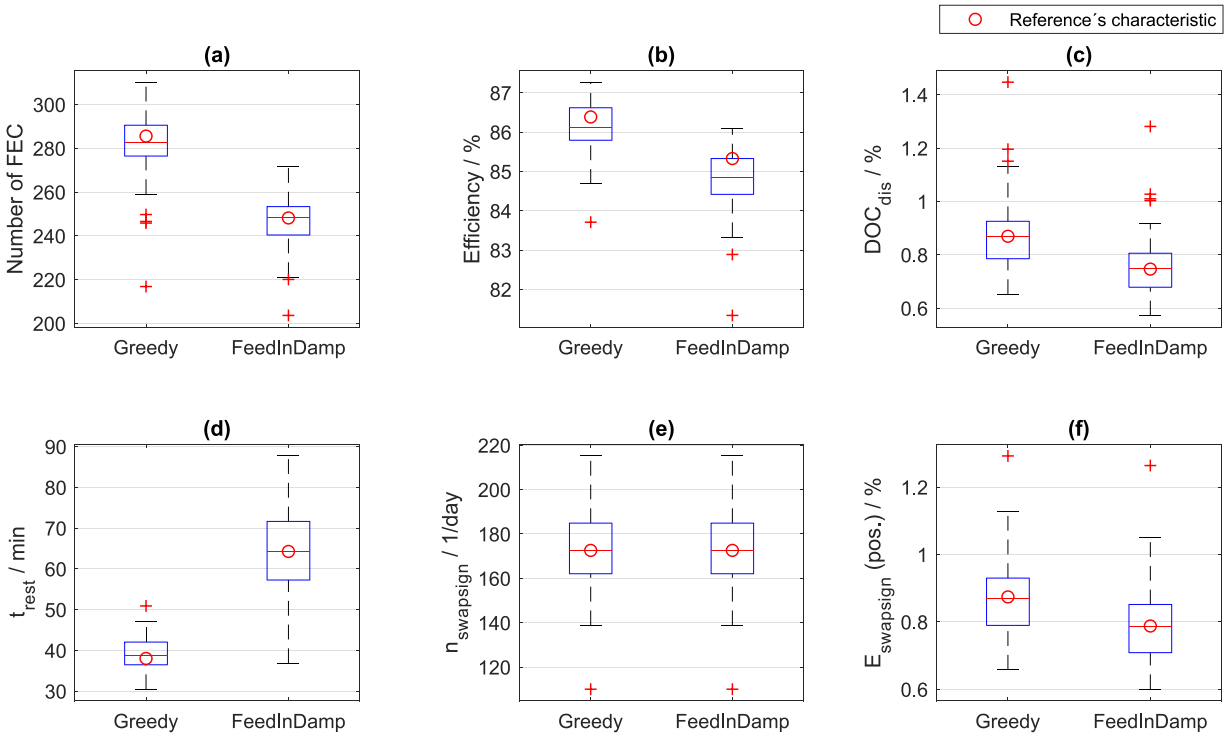

Fig. 6. Characteristics of an SCI performing BESS. The left box in each plot shows a SCI with *greedy* algorithm. The right box in each plot shows a SCI with the *feed-in damping* algorithm.

The reference profile is then chosen as the profile which has the minimum root mean squared percentage error. Thus, this profile represents the group of profiles, while maintaining its variations and peculiarities.

5. Results and discussion

The storage profile analyzer tool outputs characteristics and reference SPs which will be compared and discussed in this section. First, the characteristics of the different applications (FCR, SCI, PS) are displayed in Section 5.1. Here, a comparison is done within each application between power electronics and battery technology (FCR), operation strategies (SCI) and the three PS clusters. Afterwards, the characteristics of the reference SPs for different applications are compared to each other and thus differences in usage and load are explained (Section 5.2). Finally, exemplary days and weeks of the reference SP are shown and discussed (Section 5.3).

5.1. Characteristics of storage profiles of different applications

As described in Section 3, the simulated storage applications are FCR, SCI and PS. For each group of SPs performing one application, the different characteristics can be displayed in boxplots. These boxplots show the spread of the characteristics of a storage system performing the specific application. Each boxplot is created by using the characteristics of all the SPs. That means that for FCR five SPs, for SCI 74 SPs and for PS 36 SPs were used. Each profile contributes to each boxplot with one value. Those are the yearly number of FEC, the efficiency (η_{EES}) over the year, the average DOC in discharge direction, the average length of resting periods (t_{rest}), the average changes of sign per day ($n_{swapsign}$) and the average energy between changes of signs ($E_{swapsign}$). Each boxplot contains a red line which represents the median value. Moreover, the blue boxes display the 25th and the 75th percentiles, while the black whiskers correspond to a maximal absolute value of 2.7 times the standard deviation. The red crosses which are displayed above and underneath the boxplots show outlier outside of the box and whiskers. In addition, the red dot in each boxplot shows the value of the reference profile's characteristic (see Section 4.3). The average distance between the median value and the reference value is 2 %. The distributions of SOC, DOC in discharge direction and E-rate for all profiles and for the reference profiles of each application can be found in the appendix (Figs. B.21–B.28).

Fig. 5 displays the SPs characteristics of a BESS providing FCR. The PE units were varied as one differentiation while using the same battery technology (LFP:C). First of all, one PE unit was used (each left boxplot). Then a modular PE device was applied (each center boxplot). In addition to that, as a third boxplot, the LIB technology was varied as described in Section 3.5. Here also a modular PE device was used with a NMC:C LIB.

The first characteristic (Fig. 5 (a)) is the number of FEC within the year. Using only one PE unit leads to an increased number of FEC within the year compared to modular PE units. The high number of yearly cycles ($>$ 240 FEC in all simulations), in combination with a small DOC (Fig. 5 (c)) requires a BESS, which has a high cycle stability in the middle SOC range (see also Appendix B.21–B.23).

The efficiency (Fig. 5 (b)) can be significantly increased when using modular PE units or at least having a PE with a high part-load efficiency. Furthermore, there are almost no long resting periods (Fig. 5 (d)) and the number of sign changes (Fig. 5 (e)) is higher compared to the other applications under test. Therefore, the PE must have a high control speed to meet these requirements. The positive energy of changes of sign (Fig. 5 (f)) is a little smaller when having modular PE compared to only one device. The variation of the cell shows hardly any influence - underlining, that choosing a suitable PE design is key for improving the system's efficiency. It is worth to mention here, that battery aging was not modeled.

Fig. 6 displays the SP characteristics of a SCI BESS. The order of the six boxplot-types is the same as described before. Only the ranges of the y-axes are different as a comparison within the SCI BESS is done at this point. Here, each diagram contains one boxplot for the *greedy* operation strategy and one for the *feed-in damping* strategy (see Section 3.3). The smoothing of the load at *feed-in damping* strategy leads to a smaller number of FEC (Fig. 6 (a)), a smaller DOC (Fig. 6 (c)), a higher length of resting periods (Fig. 6 (d)) and a smaller amount of charged energy

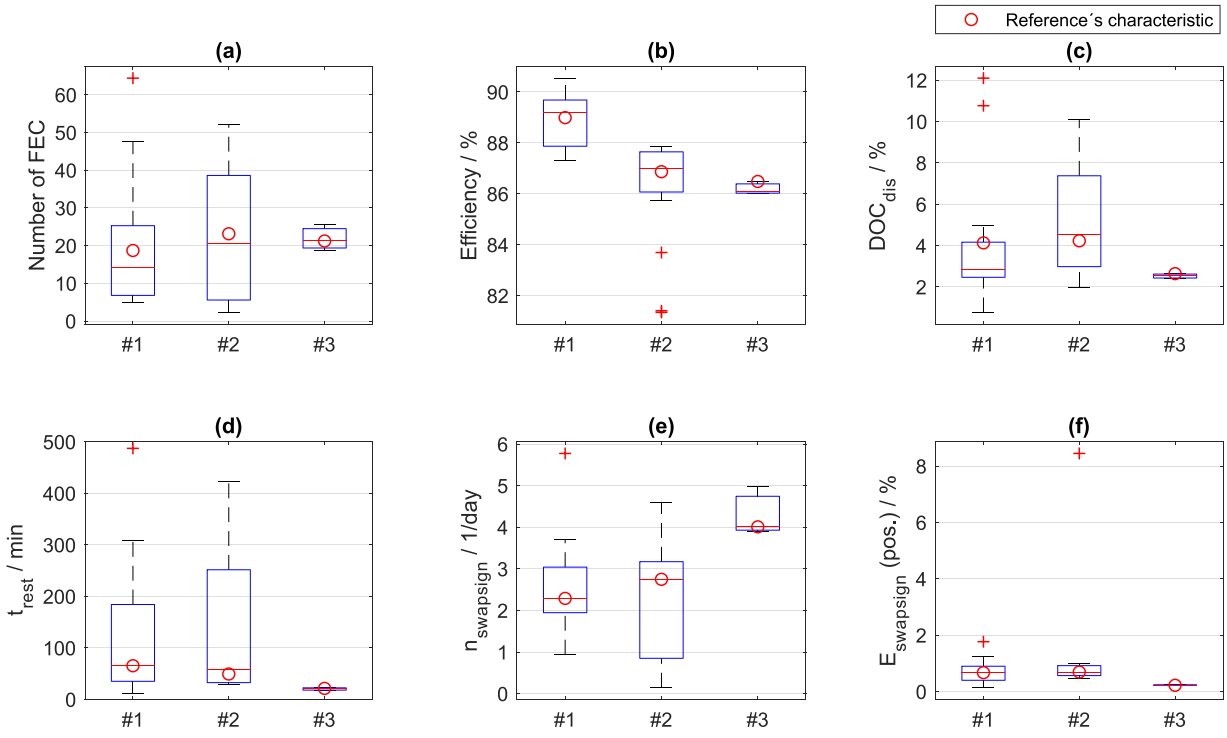

Fig. 7. Characteristics of a BESS in a PS application. The left box in each plot shows the characteristics for IP cluster 1. The box in the center for IP cluster 2 and the right one for IP cluster 3.

between sign changes (Fig. 6 (f)) compared to the *greedy* algorithm. The efficiency of the SCI BESS with *feed-in damping* algorithm is lower than with *greedy* algorithm (Fig. 6 (b)). This is due to the fact that the *feed-in damping* storage system is more often in the partial-load range where the PE has a lower efficiency.

While the lower efficiency is a disadvantage, the *feed-in damping* algorithm also leads to smaller Es-rate and lower rest times of high SOC compared to *greedy* algorithm (Appendix B.24 and B.25). Those two properties are advantages of the *feed-in damping* algorithm as longer periods of high SOC may lead to an increased calendar aging [56]. Home storage system manufacturers should take these findings into consideration and try to avoid simple rule based strategies (*greedy*). Moreover, both algorithms lead to the same number of changes of signs per day (Fig. 6 (e)), as only the time of changes vary.

The SP characteristics of a BESS in the PS application are displayed in Fig. 7. The order of the diagrams is the same but the range of y-axes is different. The three box plots in each diagram contain the SP characteristics of the three clusters of IP (see 2.4). In contrast to the other two applications (FCR and SCI) the spread of the characteristics within each group is higher. The DOC, for example, varies between 2% and 10% for cluster 2. Thus, the storage's load varies significantly depending on the industry IP. Only cluster 3 shows relatively consistent characteristics in all diagrams.

5.2. Comparison of characteristics of reference storage profiles

After the analysis of the characteristics of each application's SPs, a comparison between application SPs is done in this subsection. Therefore, the six characteristics of each reference profile are displayed in spider diagrams with the same ranges to enhance comparability (Fig. 8). For the application of FCR the reference profiles' characteristics of one PE unit and a modular PE device are displayed (top). The modular PE with an NMC:C cell is not displayed as its characteristics are almost similar to the LFP:C ones (see Fig. 5). For SCI the reference characteristics of the two algorithms are shown (middle) and the PS characteristics are displayed for the three clusters (bottom).

FCR leads to a relatively high number of cycles ($>$ 240 FEC) and small average DOCs of 0.2%. Moreover, the average resting period length is small ($<$ 10 s) and the average number of changes of sign is relatively high (600 per day). This is due to the fact, that the grid frequency fluctuates around 50 Hz and the storage system reacts quickly on frequency changes by charging or discharging the battery (see Fig. A.12). The efficiency of the storage system performing FCR with modular PE is relatively high (93%). Using only one PE device leads to a reduced efficiency of 83%. This is because of the low converter efficiency in part-load operation.

Operating the storage system for SCI leads to similar number of cycles within the year as the application of FCR. Compared to the modular PE FCR application, the efficiency is lower (approx. 85%). The average DOC is higher when performing SCI than when performing FCR (0.9% to 0.75%). The average length of resting periods is much higher when operating as a SCI BESS than when performing FCR (38 to 65 min). During winter nights, for example, the storage rests for several hours, which increases the average resting period length. Moreover, the changes of signs per day are much lower than the characteristic of FCR. 170 changes of signs per day on average still appear to be high for a SCI BESS. This is due to the fact, that during charging of the storage system by photovoltaic energy, a short increase of load or a decrease of generation (e.g. clouds) can lead to a change of sign.

Performing PS as an application leads to a much smaller number of cycles (FEC $<$ 30) and changes of sign ($n_{swapsign} < 4$ per day) compared to FCR or SCI. In contrast to that, the average DOC is higher than the other applications reference characteristics (2% to 5%). The average length of resting periods is in the same range as the SCI characteristics (20 to 65 min). Thus, it is in resting mode for a longer period of time, it does not switch between charging and discharging very often and it is discharged relatively deep, when a discharge cycle is initiated. The storage's efficiency when performing PS is between 86% and 89%. The small number of FEC, in addition to the long average length of resting periods suggests potential benefits of application stacking (multi-use) for this application. However, this requires a sufficient power load forecast.

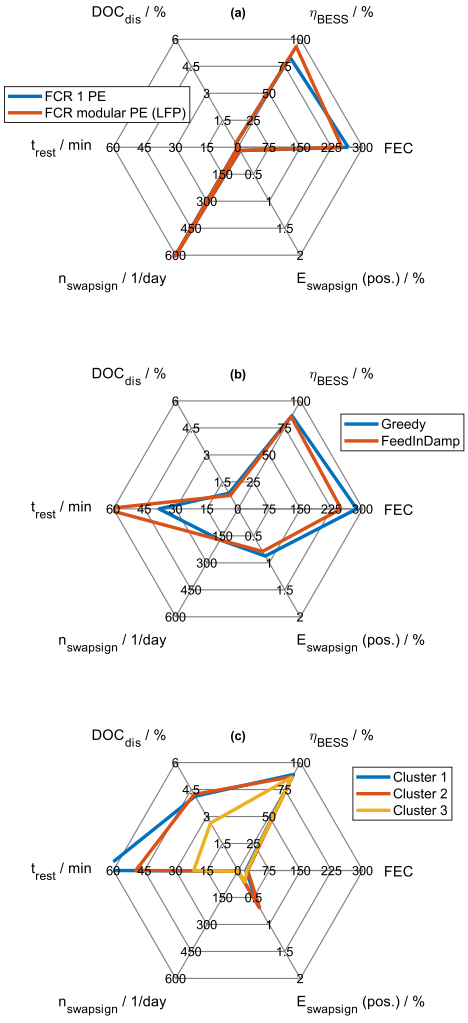

Fig. 8. Spider diagrams of the six characteristics of each reference profile (a: FCR, b: SCI and c: PS).

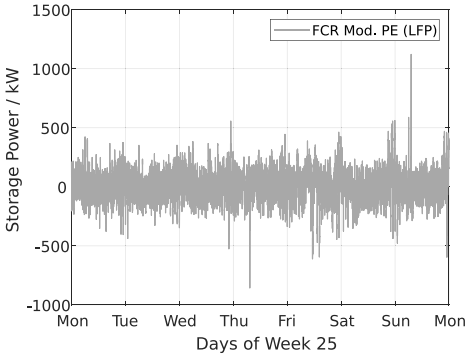

Fig. 9. Reference Storage Profile of a BESS providing FCR. Exemplary week in June.

5.3. Reference storage profiles of different applications

After the analysis of the SP characteristics and the comparison between the different storage applications, exemplary weeks of the reference profiles are shown in this Section. As described in Section 2, the FCR reference profile and the SCI reference profile exist for a whole year. The PS reference profile is for 51 weeks starting with a Monday. Appendix A shows all complete reference profiles. All reference SPs as well as the SOC at each timestep are available online free of charge, and are hosted on the servers of *TU Munich* [57].

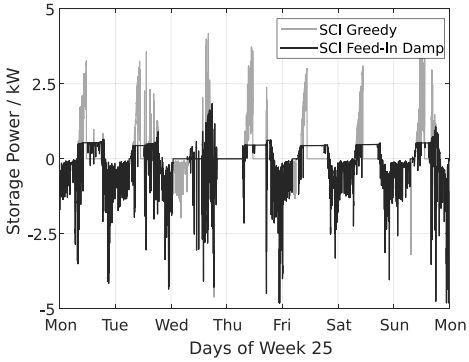

Fig. 10. Reference Storage Profile of a BESS performing SCI. Exemplary week in June.

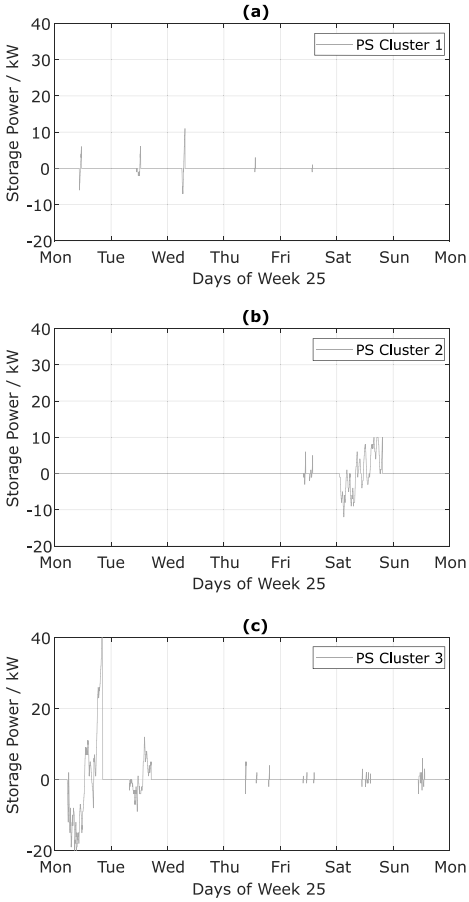

Fig. 11. Reference Storage Profile of a BESS in a PS application. Exemplary week in June. (a: Cluster 1, b: Cluster 2 and c: Cluster 3).

As an example, the 25th week of the reference profile of the FCR application with modular PE and LFP:C battery technology is displayed in Fig. 9. The diagram's y-axis shows that the maximum power in this week is around 1.1 MW. IP for this resulting reference profile was the second year frequency profile [27] (year 2014, see Section 2.1). The profile shows a high fluctuation, which results in small DOCs, a lot of changes of sign and very short resting periods (see Section 5.2). To enable a greater degree of clarity, the profiles of FCR with one PE module and with NMC:C cell (modular PE) are not displayed within the diagram. These two show a similar course with high fluctuation.

Fig. 10 depicts the 25th week of the reference profiles of the two SCI BESS with *greedy* and *feed-in damping* algorithm. Input profile for those two resulting reference profiles was the 28th household load profile from the 74 *HTW-Berlin* load profiles [28] (see Section 2.1). As this week falls in June, the storage system gets charged by the PV generation during the day. In the evening and during the night it gets discharged until the battery is empty (e.g. Thursday night). The differences in the two operating strategies were explained in Section 3.3. The *feed-in damping* profile shows the typical limitation of the energy feed into the grid, which leads to lower Es-rate for the BESS.

The reference profiles (exemplary week 25) of the three clusters of PS application are shown in Fig. 11 (a: Cluster 1, b: Cluster 2, c: Cluster 3). Here, the maximal storage power was chosen as 40 kW (see Section 3.5). As described in the previous section, the PS BESS has the fewest number of cycles and changes of signs per day. The reference SPs confirm these numbers. Moreover, the relatively long resting periods and the differences between the three clusters are visible as well. The PS threshold values for the three clusters are set to 66 kW, 83 kW and 80 kW according to the pre-processing optimization in Section 3.4.

6. Conclusion and outlook

In this paper we presented a method to create standard profiles for stationary battery energy storage systems, the results of which are available as *open data* for download. Input profiles including frequency data, industry load profiles and household load profiles are pre-processed using a normalization and clustering method. These input profiles are then transformed into storage profiles including the storage power and the state of charge using a holistic simulation framework (SimSES). This modular object-oriented tool was used to analyze three standard applications for stationary battery energy storage systems in detail and an energy management system was programmed for the different applications: (i) The energy management system for providing frequency containment reserve in SimSES was developed according to the German regulatory framework and various degrees of freedom; the efficiency was taken into account to minimize the intra-day market transactions. Moreover, a modular power electronics topology was used. (ii) In addition to a simple *greedy* algorithm, a *feed-in damping* algorithm has been implemented for a residential battery energy storage system, which charges the storage system at a low E-rate over the whole day. (iii) A two-step approach with a linear programming algorithm and SimSES was applied for an industrial peak shaving battery energy storage systems to minimize the maximum power peak value.

The results have been post-processed using a storage profile analyzer tool in order to figure out six key characteristics of the different applications. These characteristics are essential for the design of a stationary battery energy storage system. For example, for a battery energy storage system providing frequency containment reserve, the number of full equivalent cycles varies from 4 to 310 and the efficiency from 81% to 97%. Additional simulations done with SimSES for one year showed a degradation from 4% (frequency containment reserve) to 7% (peak shaving).

The *open data* available results, including storage power as well as state of charge for all reference storage profiles, with a resolution of one second can be used for comparison with other self-developed energy management systems. Furthermore other system topologies or self-developed power electronic models can be simulated with SimSES and the simulation-outcome can be assessed against the numbers presented in this paper. Scientists are encouraged to conduct aging studies or battery management system tests using the platform SimSES and data provided herein.

In order to compare both different cell chemistries as well as storage technologies, future work could focus in more detail on battery degradation. Future applications for stationary battery energy storage systems could be: buffer-storage system to reduce the peak power at (fast-) charging stations, uninterruptible power supply or island grids. As soon as the first data sets are available, it might be worthwhile to analyze these use cases more precisely.

Authors Contribution

D.K. was the principle author tasked with coordinating and writing the paper and developing SimSES; B.T. programmed the profile analyzer tool and wrote contents within the data preparation, analysis and results; S.E. helped with programming and writing the peak-shaving algorithm; A.P. helped with gathering data and the selection of the characteristics. M.M. was co-responsible for the dynamization of the input data and helped with the selection of the characteristics. Both O.B. and A.J. contributed via fruitful scientific discussions. H.H. reviewed the manuscript and was giving valuable input throughout the manuscript preparation.

Declaration of Competing Interest

The authors declare that they have no known competing financial interests or personal relationships that could have appeared to influence the work reported in this paper.

Acknowledgments

This work was financially supported by the Federal Ministry for Economic Affairs and Energy within the open_BEA project (Grant No. 03ET4072) and the EffSkalBatt project (Grant No. 03ET6148). Both projects are cared by Project Management Juelich. The responsibility for this publication rests with the authors.

Appendix A. Input and reference profiles

Fig. A.12 shows the frequency data (IP) of the whole year 2017 (top) and of one exemplary day (185) of year 2017 (bottom). The Figs. A.13–A.20 show the complete reference profiles. The FCR reference profile and the SCI reference profile are for a whole year. The PS reference profile are for 51 weeks starting with a Monday. All reference

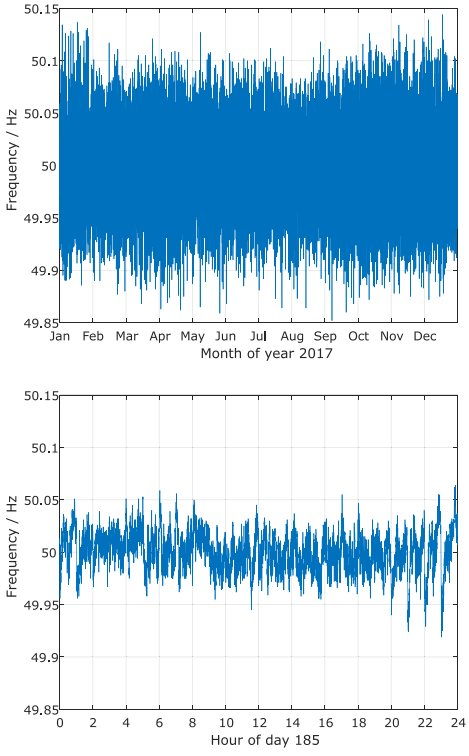

Fig. A.12. Sample sections of frequency data of the whole year 2017 (top) and of one exemplary day (185) of year 2017 (bottom).

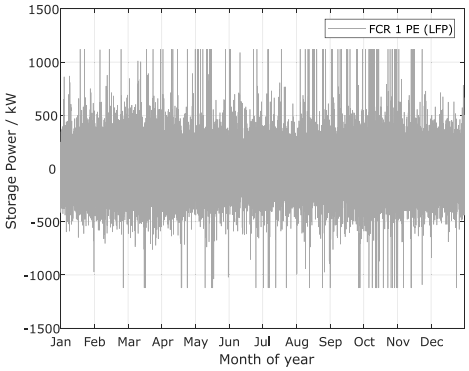

Fig. A.13. Yearly reference profile of a simulated BESS with one PE unit and a LFP:C cell providing FCR.

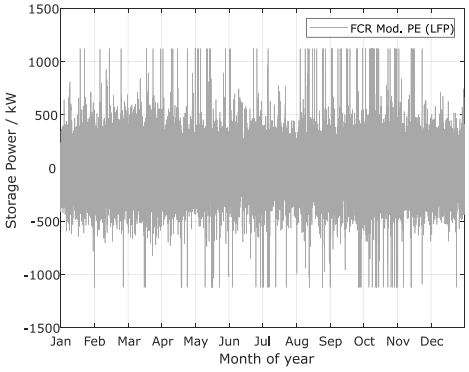

Fig. A.14. Yearly reference profile of a simulated BESS with three modular PE units and a LFP:C cell providing FCR.

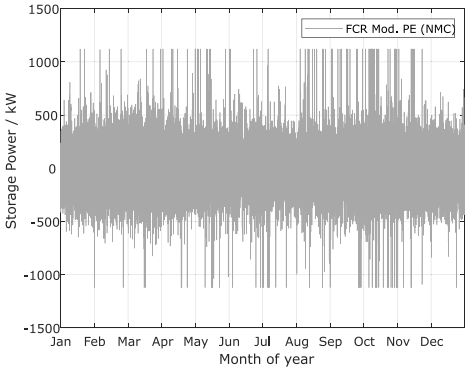

Fig. A.15. Yearly reference profile of a simulated BESS with three modular PE units and a NMC:C cell providing FCR.

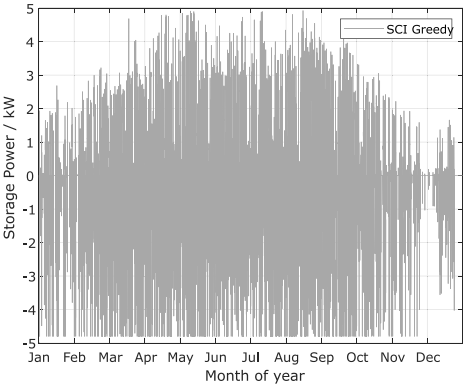

Fig. A.16. Yearly reference profile of a BESS for SCI with one PE unit and a LFP:C cell with the *greedy* algorithm.

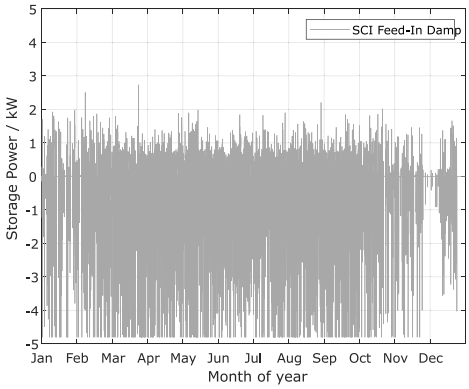

Fig. A.17. Yearly reference profile of a BESS for SCI with one PE unit and a LFP:C cell with the *feed-in damping* algorithm.

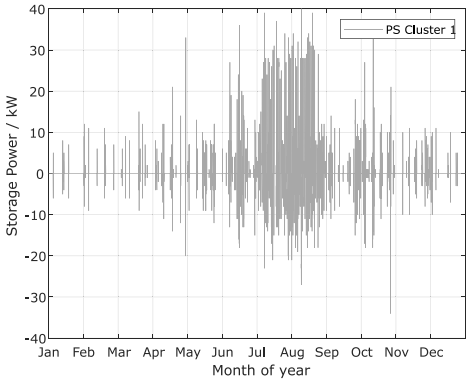

Fig. A.18. Yearly reference profile of a BESS in the application of PS with one PE unit and a LFP:C cell in cluster 1.

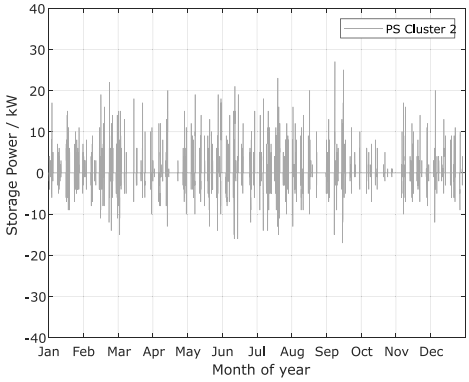

Fig. A.19. Yearly reference profile of a BESS in the application of PS with one PE unit and a LFP:C cell in cluster 2.

SP as well as the SOC at each timestep can be downloaded in a MATLAB R2019a® data format (*mat*) or hierarchical data format (*hdf5*) from the servers of TU Munich [57].

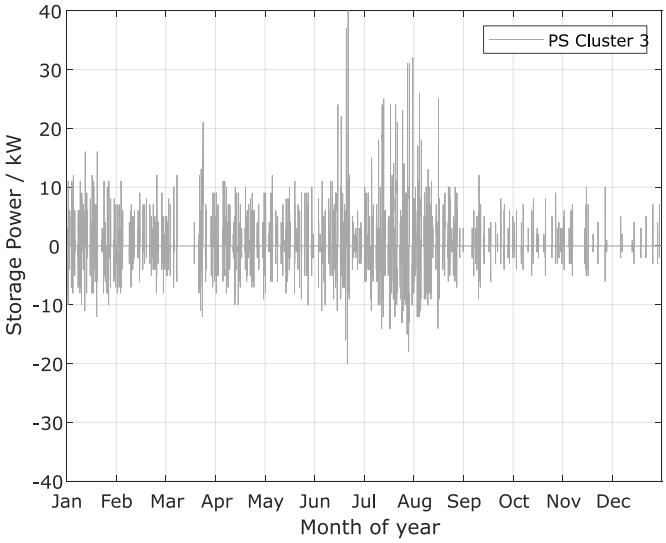

Fig. A.20. Yearly reference profile of a BESS in the application of PS with one PE unit and a LFP:C cell in cluster 3.

Appendix B. Further analysis with SimSES

B1. Frequency containment reserve

Figs. B.21, B.22 and B.23 shows additional analysis for the simulations of a BESS providing FCR. The left-hand plots (a, d) show the distribution of the SOC, the middle one (b, e) show the distribution of the DOC and the right-hand plots (c, f) show the distribution of the E-rate. The three plots at the top (a-c) at each figure show the mean results of all 5 simulations. The three plots at the bottom (d-f) show at each figure the result for the reference profile. All plots have a logarithmic y-axis.

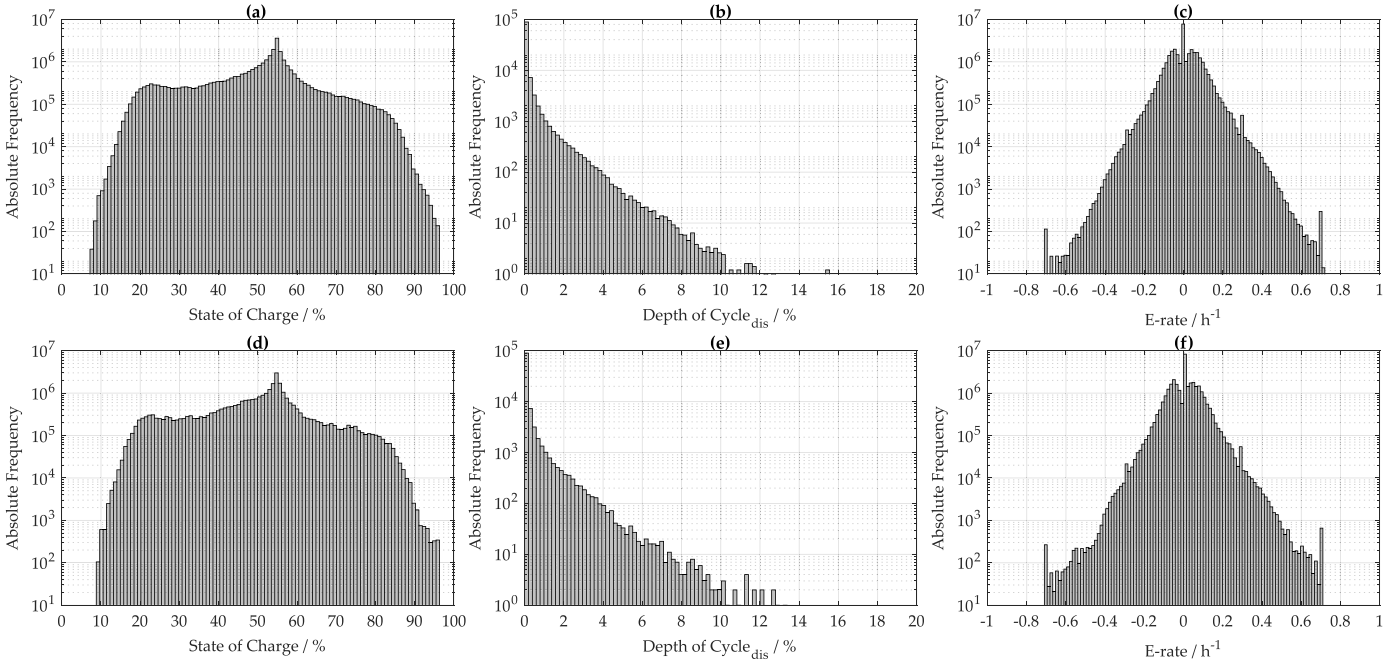

Fig. B.21. Additional analysis, SOC (a, d), DOC (b, e) and E-rate (c, f), of a simulated BESS with one PE unit and a LFP:C cell providing FCR. The three plots at the top (a-c) show the mean results of all 5 simulations. The three plots at the bottom (d-f) show the result for the reference profile.

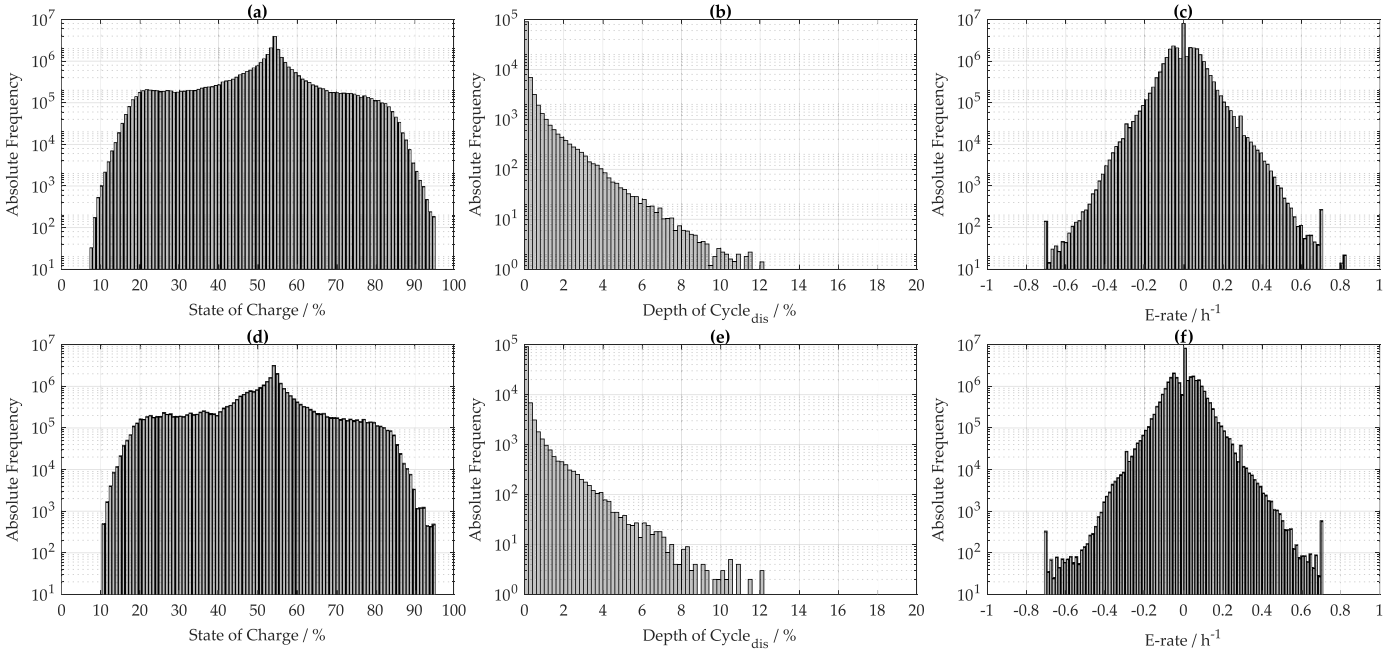

Fig. B.22. Additional analysis, SOC (a, d), DOC (b, e) and E-rate (c, f), of a simulated BESS with three modular PE units and a NMC:C cell providing FCR. The three plots at the top (a-c) show the mean results of all 5 simulations. The three plots at the bottom (d-f) show the result for the reference profile.

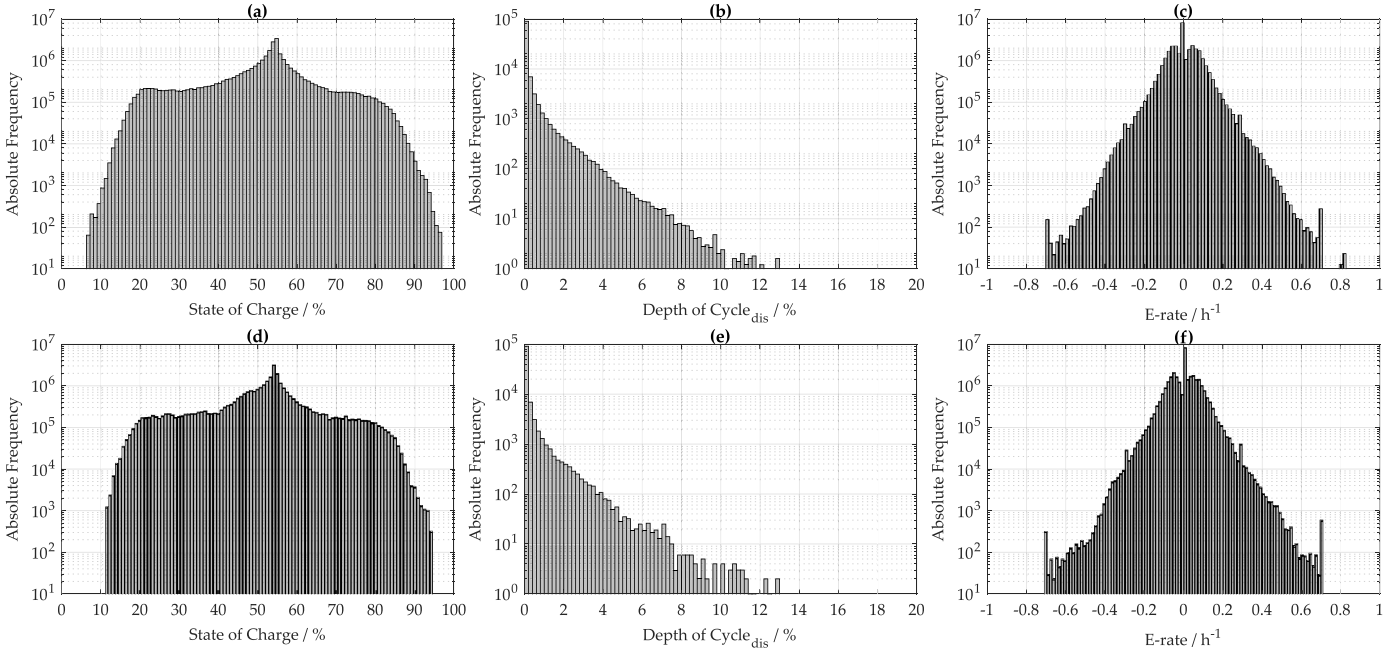

Fig. B.23. Additional analysis, SOC (a, d), DOC (b, e) and E-rate (c, f), of a simulated BESS with three modular PE units and a LFP:C cell providing FCR. The three plots at the top (a-c) show the mean results of all 5 simulations. The three plots at the bottom (d-f) show the result for the reference profile.

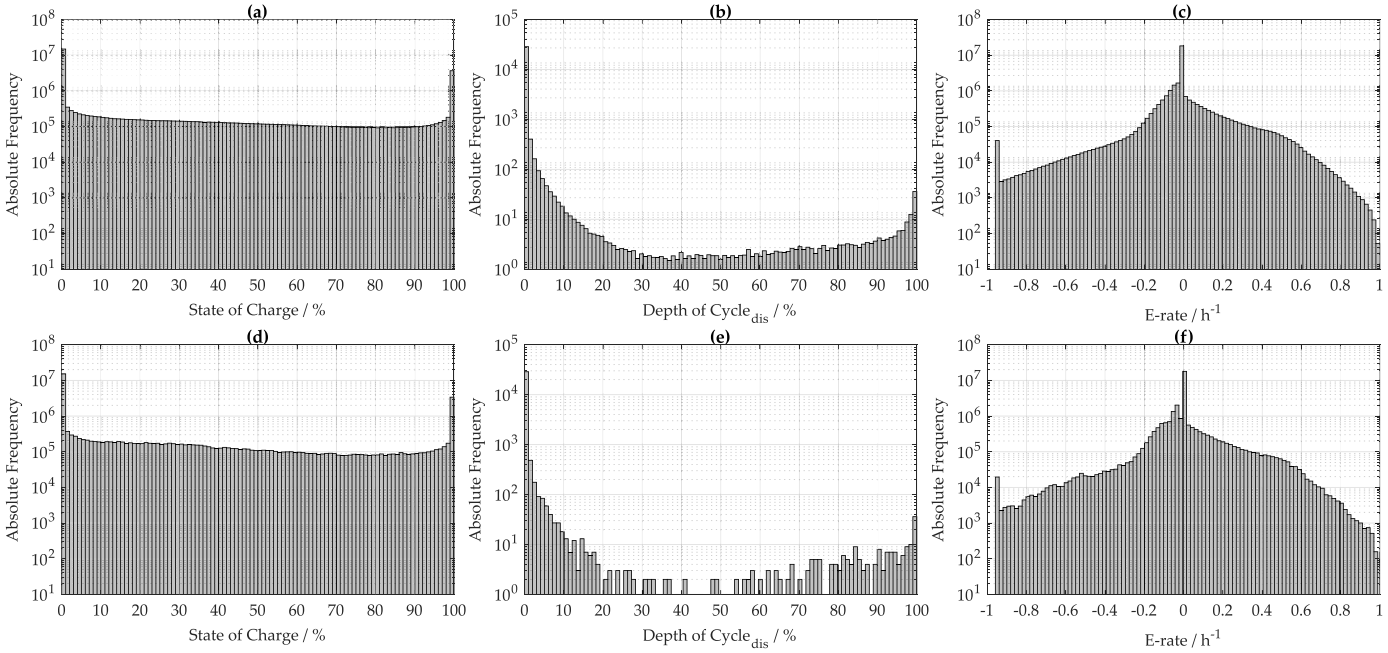

Fig. B.24. Additional analysis, SOC (a, d), DOC (b, e) and E-rate (c, f), of a SCI BESS with one PE unit and a LFP:C cell with the *greedy* algorithm. The three plots at the top (a-c) show the mean results of all 74 simulations. The three plots at the bottom (d-f) show the result for the reference profile.

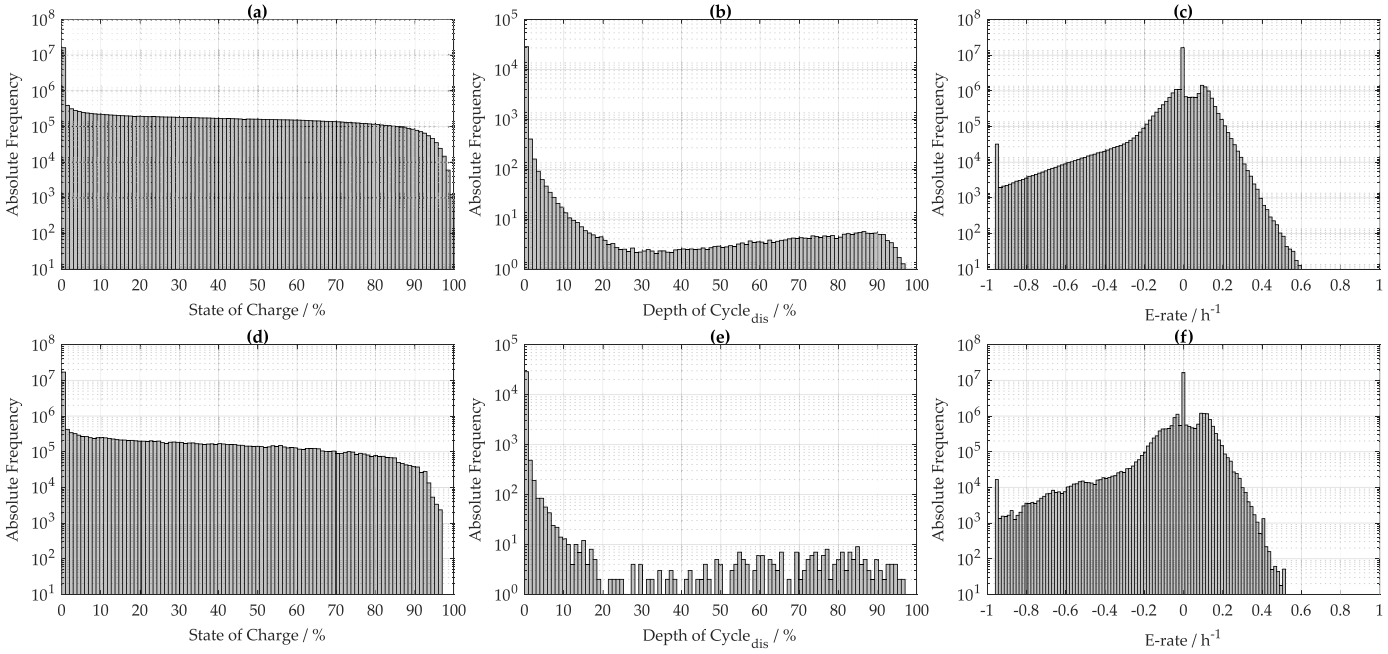

Fig. B.25. Additional analysis, SOC (a, d), DOC (b, e) and E-rate (c, f), of a SCI BESS with one PE unit and a LFP:C cell with the *feed-in damping* algorithm. The three plots at the top (a-c) show the mean results of all 74 simulations. The three plots at the bottom (d-f) show the result for the reference profile.

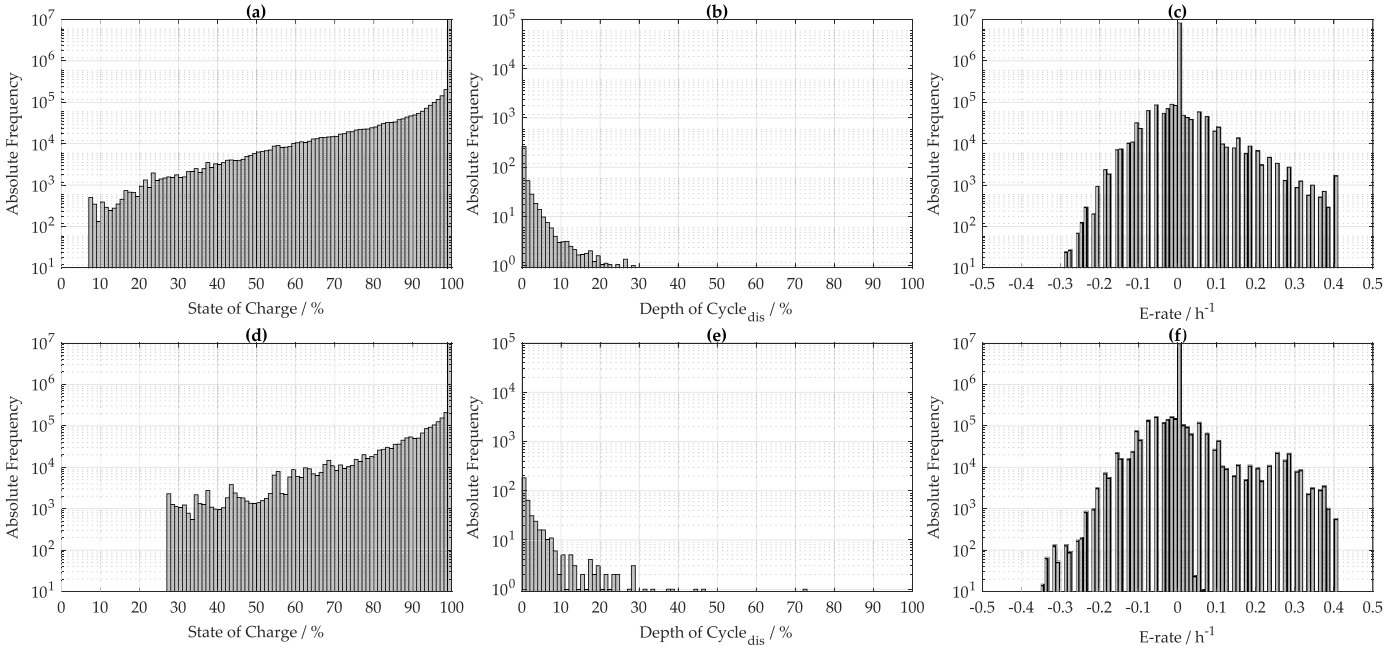

Fig. B.26. Additional analysis, SOC (a, d), DOC (b, e) and E-rate (c, f), of a BESS in the application of PS with one PE unit and a LFP:C cell in cluster 1. The three plots at the top (a-c) show the mean results of all simulations in cluster 1. The three plots at the bottom (d-f) show the result for the reference profile in cluster 1.

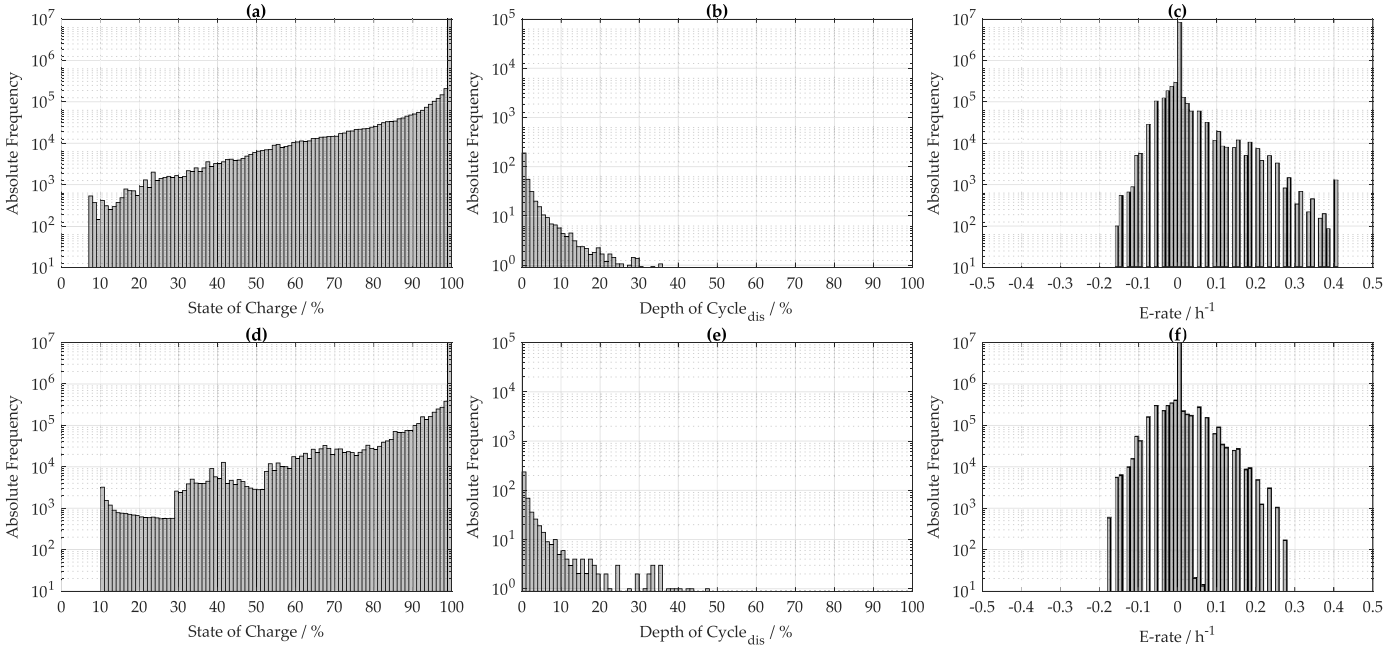

Fig. B.27. Additional analysis, SOC (a, d), DOC (b, e) and E-rate (c, f), of a BESS in the application of PS with one PE unit and a LFP:C cell in cluster 2. The three plots at the top (a-c) show the mean results of all simulations in cluster 2. The three plots at the bottom (d-f) show the result for the reference profile in cluster 2.

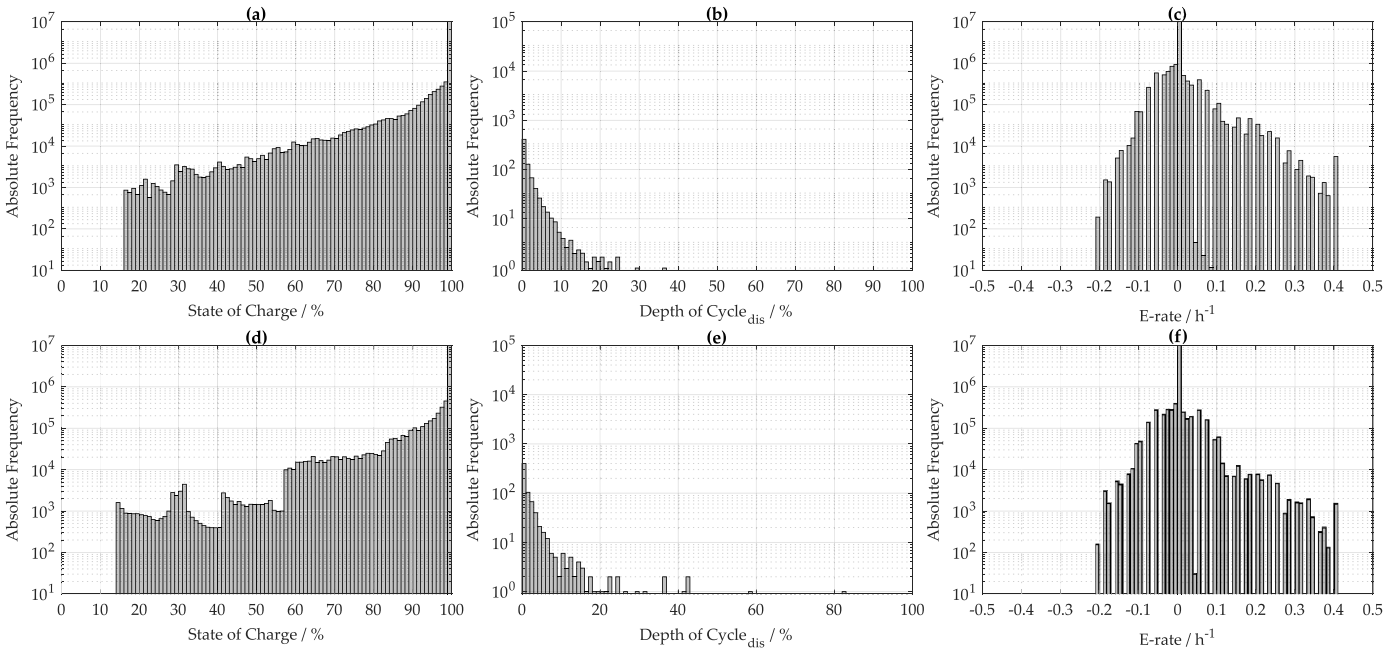

Fig. B.28. Additional analysis, SOC (a, d), DOC (b, e) and E-rate (c, f), of a BESS in the application of PS with one PE unit and a LFP:C cell in cluster 3. The three plots at the top (a-c) show the mean results of all simulations in cluster 3. The three plots at the bottom (d-f) show the result for the reference profile in cluster 3.

B2. Residential photovoltaic battery storage system

Figs. B.24 and B.25 shows additional analysis for the simulations of a SCI BESS. The left-hand plots (a, d) show the distribution of the SOC, the middle one (b, e) show the distribution of the DOC and the right-hand plots (c, f) show the distribution of the E-rate. The three plots at the top (a-c) at each figure show the mean results of all 74 simulations. The three plots at the bottom (d-f) show at each figure the result for the reference profile. All plots have a logarithmic y-axis.

B3. Peak shaving storage system

Figs. B.26, B.27 and B.28 shows additional analysis for the simulations of a BESS in the application of PS. The left-hand plots show the distribution of the SOC, the middle one (b, e) show the distribution of the DOC and the right-hand plots (c, f) show the distribution of the E-rate. The three plots at the top (a-c) at each figure show the mean results of all simulations in the respective cluster. The three plots at the bottom (d-f) show at each figure the result for the reference profile in the respective cluster. All plots have a logarithmic y-axis.

Supplementary material

Supplementary material associated with this article can be found, in the online version, at doi:10.1016/j.est.2019.101077

References

[1] TEAM CONSULT G.P.E. GmbH, Bedeutung der energiespeicherbranche für das energiesystem und die gesamtwirtschaft in deutschland (in german): pressekonferenz messe düsseldorf gmbh & bves bundesverband energiespeicher e. v. zur energy storage Europe 2018, 13.03.2018, https://www.bves.de/wp-content/uploads/2018/03/PK_ESE_Praesentation_2018.pdf.

[2] J. Eyer, G. Corey, Energy Storage for the Electricity Grid: benefits and Market Potential Assessment Guide: a Study for the Doe Energy Storage Systems Program.

[3] H. Hesse, M. Schimpe, D. Kucevic, A. Jossen, Lithium-ion battery storage for the grid—a review of stationary battery storage system design tailored for applications in modern power grids, Energies 10 (12) (2017) 2107, https://doi.org/10.3390/en10122107.

[4] M. Resch, J. Bühler, M. Klausen, A. Sumper, Impact of operation strategies of large scale battery systems on distribution grid planning in germany, Renew. Sustain. Energy Rev. 74 (2017) 1042–1063, https://doi.org/10.1016/j.rser.2017.02.075.

[5] B. Diouf, R. Pode, Potential of lithium-ion batteries in renewable energy, Renew Energy 76 (2015) 375–380, https://doi.org/10.1016/j.renene.2014.11.058.

[6] O. Palizban, K. Kauhaniemi, Energy storage systems in modern grids—matrix of technologies and applications, J. Energy Storage 6 (2016) 248–259, https://doi.org/10.1016/j.est.2016.02.001.

[7] B. Dunn, H. Kamath, J.-M. Tarascon, Electrical energy storage for the grid: a battery of choices, Science 334 (6058) (2011) 928–935, https://doi.org/10.1126/science.1212741.

[8] T. Weitzel, C.H. Glock, Energy management for stationary electric energy storage systems: a systematic literature review, Eur. J. Oper. Res. (2017), https://doi.org/10.1016/j.ejor.2017.06.052.

[9] C.K. Das, O. Bass, G. Kothapalli, T.S. Mahmoud, D. Habibi, Overview of energy storage systems in distribution networks: placement, sizing, operation, and power quality, Renew. Sustain. Energy Rev. 91 (2018) 1205–1230, https://doi.org/10.1016/j.rser.2018.03.068.

[10] G. Carpinelli, F. Mottola, C. Noce, A. Russo, P. Varilone, A new hybrid approach using the simultaneous perturbation stochastic approximation method for the optimal allocation of electrical energy storage systems, Energies 11 (6) (2018) 1505, https://doi.org/10.3390/en11061505.

[11] A. Oudalov, D. Chartouni, C. Ohler, Optimizing a battery energy storage system for primary frequency control, IEEE Trans. Power Syst. 22 (3) (2007) 1259–1266, https://doi.org/10.1109/TPWRS.2007.901459.

[12] R. Hollinger, L.M. Diazgranados, F. Braam, T. Erge, G. Bopp, B. Engel, Distributed solar battery systems providing primary control reserve, IET Renew. Power Gener. 10 (1) (2016).

[13] J. Fleer, P. Stenzel, Impact analysis of different operation strategies for battery energy storage systems providing primary control reserve, J. Energy Storage 8 (2016) 320–338, https://doi.org/10.1016/j.est.2016.02.003.

[14] A. Zeh, M. Müller, M. Naumann, H. Hesse, A. Jossen, R. Witzmann, Fundamentals of using battery energy storage systems to provide primary control reserves in germany, Batteries 2 (3) (2016) 29, https://doi.org/10.3390/batteries2030029.

[15] Y.J.A. Zhang, C. Zhao, W. Tang, S.H. Low, Profit-maximizing planning and control of battery energy storage systems for primary frequency control, IEEE Trans Smart Grid 9 (2) (2018) 712–723, https://doi.org/10.1109/TSG.2016.2562672.

[16] J. Münderlein, M. Steinhoff, S. Zurmühlen, D.U. Sauer, Analysis and evaluation of operations strategies based on a large scale 5 mw and 5 mwh battery storage system, J. Energy Storage 24 (2019) 100778, https://doi.org/10.1016/j.est.2019.100778.

[17] M. Naumann, R.C. Karl, C.N. Truong, A. Jossen, H.C. Hesse, Lithium-ion battery cost analysis in pv-household application. 9th International Renewable Energy Storage Conference, IRES 2015 73, 2015, pp. 37–47, https://doi.org/10.1016/j.egypro.2015.07.555.

[18] F. Cucchiella, I. D'Adamo, M. Gastaldi, Photovoltaic energy systems with battery storage for residential areas: an economic analysis, J. Clean. Prod. 131 (2016) 460–474, https://doi.org/10.1016/j.jclepro.2016.04.157.

[19] C.N. Truong, M. Naumann, R.C. Karl, M. Müller, A. Jossen, H.C. Hesse, Economics of residential photovoltaic battery systems in germany: the case of teslas powerwall, Batteries 2 (2) (2016) 14, https://doi.org/10.3390/batteries2020014.

[20] H. Hesse, R. Martins, P. Musilek, M. Naumann, C. Truong, A. Jossen, Economic optimization of component sizing for residential battery storage systems, Energies 10 (7) (2017) 835, https://doi.org/10.3390/en10070835.

[21] J. Weniger, T. Tjaden, V. Quaschning, Sizing of residential pv battery systems. 9th International Renewable Energy Storage Conference, IRES 2015 46, 2014, pp. 78–87, https://doi.org/10.1016/j.egypro.2014.01.160.
[22] R. Tang, B. Yildiz, P.H. Leong, A. Vassallo, J. Dore, Residential battery sizing model using net meter energy data clustering, Appl. Energy 251 (2019) 113324, https://doi.org/10.1016/j.apenergy.2019.113324.
[23] F.M. Vieira, P.S. Moura, A.T. de Almeida, Energy storage system for self-consumption of photovoltaic energy in residential zero energy buildings, Renew Energy 103 (2017) 308–320, https://doi.org/10.1016/j.renene.2016.11.048.
[24] R. Martins, H. Hesse, J. Jungbauer, T. Vorbuchner, P. Musilek, Optimal component sizing for peak shaving in battery energy storage system for industrial applications, Energies 11 (8) (2018) 2048, https://doi.org/10.3390/en11082048.
[25] H. Dagdougui, N. Mary, A. Beraud-Sudreau, L. Dessaint, Power management strategy for sizing battery system for peak load limiting in a university campus. 2016 IEEE Smart Energy Grid Engineering (SEGE), IEEE, 21.08.2016 - 24.08.2016, pp. 308–312, https://doi.org/10.1109/SEGE.2016.7589542.
[26] E. Telaretti, L. Dusonchet, Battery storage systems for peak load shaving applications: Part 2: economic feasibility and sensitivity analysis. 2016 IEEE 16th International Conference on Environment and Electrical Engineering (EEEIC), IEEE, 07.06.2016 - 10.06.2016, pp. 1–6, https://doi.org/10.1109/EEEIC.2016.7555795.
[27] 50Hertz Transmission GmbH, Archiv netzfrequenz (in german): daten der entso-e netzfrequenz, 2019, https://www.50hertz.com/de/Transparenz/Kennzahlen/Regelenergie/ArchivRegelenergie/ArchivNetzfrequenz.
[28] T. Tjaden, J. Bergner, J. Weniger, V. Quaschning, Repräsentative elektrische lastprofile für wohngebäude in deutschland auf 1-sekündiger datenbasis (in German), https://pvspeicher.htw-berlin.de/daten/.
[29] A. Zeh, R. Witzmann, Operational strategies for battery storage systems in low-voltage distribution grids to limit the feed-in power of roof-mounted solar power systems, Energy Procedia 46 (2014) 114–123, https://doi.org/10.1016/j.egypro.2014.01.164.
[30] P. Keil, A. Jossen, Charging protocols for lithium-ion batteries and their impact on cycle life—an experimental study with different 18650 high-power cells, J. Energy Storage 6 (2016) 125–141, https://doi.org/10.1016/j.est.2016.02.005.
[31] G. Ning, B. Haran, B.N. Popov, Capacity fade study of lithium-ion batteries cycled at high discharge rates, J Power Source. 117 (1–2) (2003) 160–169, https://doi.org/10.1016/S0378-7753(03)00029-6.
[32] B. Everitt, Cluster analysis, in: Wiley series in probability and statistics, Wiley, Chichester West Sussex U.K., 2011.
[33] A. Al-Wakeel, J. Wu, K-Means based cluster analysis of residential smart meter measurements, 9th International Renewable Energy Storage Conference, IRES 2015 88 (2016) 754–760, https://doi.org/10.1016/j.egypro.2016.06.066.
[34] G. Le Ray, P. Pinson, Online adaptive clustering algorithm for load profiling, Sustain. Energy Grids Netw. 17 (2019) 100181, https://doi.org/10.1016/j.segan.2018.100181.
[35] G.J. Tsekouras, N.D. Hatziargyriou, E.N. Dialynas, Two-stage pattern recognition of load curves for classification of electricity customers, IEEE Trans. Power Syst. 22 (3) (2007) 1120–1128, https://doi.org/10.1109/TPWRS.2007.901287.
[36] F. McLoughlin, A. Duffy, M. Conlon, A clustering approach to domestic electricity load profile characterisation using smart metering data, Appl. Energy 141 (2015) 190–199, https://doi.org/10.1016/j.apenergy.2014.12.039.
[37] T. Räsänen, D. Voukantsis, H. Niska, K. Karatzas, M. Kolehmainen, Data-based method for creating electricity use load profiles using large amount of customer-specific hourly measured electricity use data, Appl. Energy 87 (11) (2010) 3538–3545, https://doi.org/10.1016/j.apenergy.2010.05.015.
[38] M. Naumann, C.N. Truong, M. Schimpe, D. Kucevic, A. Jossen, H.C. Hesse, Simses: Software for techno-economic simulation of stationary energy storage systems. International ETG Congress 2017, in: ETG-Fachbericht, VDE Verlag, Berlin and Offenbach, 2017, pp. 442–447.
[39] Deutsche Übertragungsnetzbetreiber, Eckpunkte und freiheitsgrade bei erbringung von primaerregelleistung (in German): Leitfaden für anbieter von primaerregelleistung, https://www.regelleistung.net/ext/static/prequalification?lang=en.
[40] Deutsche Übertragungsnetzbetreiber, Anforderungen an die speicherkapazitaet bei batterien für die primaerregelleistung (in German), https://www.bves.de/wp-content/uploads/2015/08/2015_08_26_Anforderungen_Speicherkapazitaet_Batterien_PRL.pdf.
[41] BVES, Beschränkung der ünb für speicher im regelenergiemarkt ist rechtswidrig (in German), 09.05., 2019, https://www.bves.de/uenb_rechtswidrige_blockade/.
[42] German Federal Office of Justice, Stromnetzentgeltverordnung (in German): Stromnev, 2005-07-25, https://www.gesetze-im-internet.de/stromnev/BJNR222500005.html.
[43] S. Englberger, H.C. Hesse, C.N. Truong, A. Jossen, Autonomous versus Coordinated Control of Residential Energy Storage Systems - Monitoring Profit, Battery Aging, and System Efficiency, in: D. Schulz (Ed.), NEIS 2018, VDE VERLAG GMBH, Berlin, 2019, pp. 1–7.
[44] S. Englberger, H. Hesse, D. Kucevic, A. Jossen, A techno-economic analysis of vehicle-to-building: battery degradation and efficiency analysis in the context of coordinated electric vehicle charging, Energies 12 (5) (2019) 955, https://doi.org/10.3390/en12050955.
[45] D. Kucevic, C.N. Truong, A. Jossen, H.C. Hesse, Lithium-ion Battery Storage Design for Buffering Fast Charging Stations for Battery Electric Vehicles and Electric Buses, in: D. Schulz (Ed.), NEIS 2018, VDE VERLAG GMBH, Berlin, 2019, pp. 1–6.
[46] Murata, Data sheet of Sony fortelion us26650ftc1 battery cell, 2017.
[47] A.-I. Stan, M. Swierczynski, D.-I. Stroe, R. Teodorescu, S.J. Andreasen, Lithium ion battery chemistries from renewable energy storage to automotive and back-up power applications — an overview. 2014 International Conference on Optimization of Electrical and Electronic Equipment (OPTIM), IEEE, 2014, pp. 713–720, https://doi.org/10.1109/OPTIM.2014.6850936.
[48] M. Müller, L. Viernstein, C.N. Truong, A. Eiting, H.C. Hesse, R. Witzmann, A. Jossen, Evaluation of grid-level adaptability for stationary battery energy storage system applications in europe, J. Energy Storage 9 (2017) 1–11, https://doi.org/10.1016/j.est.2016.11.005.
[49] M. Naumann. Techno-economic evaluation of stationary battery energy storage systems with special consideration of aging, Technical University of Munich, Munich, 2018. Phd thesis.
[50] Molicel, Product data sheet model ihr-18650a.
[51] S.F. Schuster. Reuse of Automotive Lithium-Ion Batteries: An Assessment from the Cell Aging Perspective, Universitätsbibliothek der TU München, München, 2016. Dissertation.
[52] G. Notton, V. Lazarov, L. Stoyanov, Optimal sizing of a grid-connected pv system for various pv module technologies and inclinations, inverter efficiency characteristics and locations, Renew Energy 35 (2) (2010) 541–554, https://doi.org/10.1016/j.renene.2009.07.013.
[53] M. Schimpe, M. Naumann, N. Truong, H.C. Hesse, S. Santhanagopalan, A. Saxon, A. Jossen, Energy efficiency evaluation of a stationary lithium-ion battery container storage system via electro-thermal modeling and detailed component analysis, Appl. Energy 210 (2018) 211–229, https://doi.org/10.1016/j.apenergy.2017.10.129.
[54] J. Hoppmann, J. Volland, T.S. Schmidt, V.H. Hoffmann, The economic viability of battery storage for residential solar photovoltaic systems – a review and a simulation model, Renew. Sustain. Energy Rev. 39 (2014) 1101–1118, https://doi.org/10.1016/j.rser.2014.07.068.
[55] S.F. Schuster, T. Bach, E. Fleder, J. Müller, M. Brand, G. Sextl, A. Jossen, Nonlinear aging characteristics of lithium-ion cells under different operational conditions, J. Energy Storage 1 (2015) 44–53, https://doi.org/10.1016/j.est.2015.05.003.
[56] M. Naumann, M. Schimpe, P. Keil, H.C. Hesse, A. Jossen, Analysis and modeling of calendar aging of a commercial lifepo4/graphite cell, J. Energy Storage 17 (2018) 153–169, https://doi.org/10.1016/j.est.2018.01.019.
[57] D. Kucevic, B. Tepe, S. Englberger, A. Parlikar, M. Muehlbauer, O. Bohlen, A. Jossen, H. Hesse, Standard battery energy storage system profiles: dataset, doi:10.14459/2019mp1510254.